OXFORD

Human Molecular Genetics, 2015, Vol. 24, No. 25 7265–7285

doi: 10.1093/hmg/ddv426
Advance Access Publication Date: 12 October 2015
Original Article

ORIGINAL ARTICLE

A role for Kalirin-7 in corticostriatal synaptic dysfunction in Huntington's disease

Mar Puigdellívol[1,2,3], Marta Cherubini[1,2,3,†], Verónica Brito[1,2,3,†], Albert Giralt[1,2,3], Núria Suelves[1,2,3], Jesús Ballesteros[4], Alfonsa Zamora-Moratalla[4], Eduardo D. Martín[4], Betty A. Eipper[5], Jordi Alberch[1,2,3] and Silvia Ginés[1,2,3,*]

[1]Departament de Biologia Cellular, Immunologia i Neurociències, Facultat de Medicina, Universitat de Barcelona, Barcelona, Spain, [2]Institut d'Investigacions Biomèdiques August Pi i Sunyer (IDIBAPS), Barcelona, Spain, [3]CIBERNED, Madrid, Spain, [4]Laboratory of Neurophysiology and Synaptic Plasticity, Albacete Science and Technology Park (PCYTA), Institute for Research in Neurological Disabilities (IDINE), University of Castilla-La Mancha, Albacete, Spain and [5]Department of Neuroscience, University of Connecticut Health Center, Farmington, CT, USA

*To whom correspondence should be addressed at: Universitat de Barcelona, Casanova 143, E-08036 Barcelona, Spain. Tel: +34 934035284; Fax: +34 934021907; Email: silviagines@ub.edu

Abstract

Cognitive dysfunction is an early clinical hallmark of Huntington's disease (HD) preceding the appearance of motor symptoms by several years. Neuronal dysfunction and altered corticostriatal connectivity have been postulated to be fundamental to explain these early disturbances. However, no treatments to attenuate cognitive changes have been successful: the reason may rely on the idea that the temporal sequence of pathological changes is as critical as the changes *per se* when new therapies are in development. To this aim, it becomes critical to use HD mouse models in which cognitive impairments appear prior to motor symptoms. In this study, we demonstrate procedural memory and motor learning deficits in two different HD mice and at ages preceding motor disturbances. These impairments are associated with altered corticostriatal long-term potentiation (LTP) and specific reduction of dendritic spine density and postsynaptic density (PSD)-95 and spinophilin-positive clusters in the cortex of HD mice. As a potential mechanism, we described an early decrease of Kalirin-7 (Kal7), a guanine-nucleotide exchange factor for Rho-like small GTPases critical to maintain excitatory synapse, in the cortex of HD mice. Supporting a role for Kal7 in HD synaptic deficits, exogenous expression of Kal7 restores the reduction of excitatory synapses in HD cortical cultures. Altogether, our results suggest that cortical dysfunction precedes striatal disturbances in HD and underlie early corticostriatal LTP and cognitive defects. Moreover, we identified diminished Kal7 as a key contributor to HD cortical alterations, placing Kal7 as a molecular target for future therapies aimed to restore corticostriatal function in HD.

Introduction

Basal ganglia dysfunction is a clear hallmark of Huntington's disease (HD) involved in the classical motor disturbances. However, it is patent that HD encompasses more than motor deficits, with evidence of cognitive dysfunction years before chorea symptoms appear. In this view, it has been suggested that functional and morphological changes in key brain areas involved in cognitive processes such as the neocortex could precede alterations in the striatum and be the initial trigger of striatal pathology and late-stage motor symptoms (1–3). Thus, cognitive deficits

[†]The authors wish it to be known that, in their opinion, the second two authors should be regarded as joint Second Authors.

Received: June 30, 2015. **Revised and Accepted:** October 5, 2015

manifested by HD patients such as impaired sensory discrimination, learning, memory, planning and decision making have been related with neocortical dysfunction (4–9) while specific thinning of the neocortex has been demonstrated in stages I–II of HD individuals (10,11). Interestingly, deficient cortical function evidenced by decreased glutamate receptor-mediated currents (12), impaired learning-dependent cortical plasticity (2,13) and altered excitability of cortical pyramidal neurons (1,14) has also been reported in different HD mouse models at early disease stages.

Changes in the structure, location or number of dendritic spines, which represent the site of most glutamatergic synapses in the brain, have been critically involved in the synaptic deficits of different neurological disorders (15–18). Thus, in symptomatic transgenic HD mice (19,20) and in HD postmortem human brain (21–23), reduced dendritic spines and altered dendritic morphology have been reported in cortical pyramidal neurons and striatal neurons, suggesting that cognitive deficits in HD could be driven by deficiency of corticostriatal connectivity due to dendritic spine alterations. However, the molecular mechanisms underlying these changes are poorly understood. Dendritic spine dynamics are dependent on neuronal activity through modulation of the actin cytoskeleton by Rho-family GDP/GTP exchange factors (Rho-GEFs) and the corresponding GTPase-activating proteins (24–27). Kalirin-7 (Kal7), a brain-specific Rho-GEF for Rac-like GTPases, is enriched in the dendritic spines of neuronal populations where it plays a critical role in structural and functional plasticity of excitatory synapses (28–31). Accordingly, Kal7-positive clusters were found to overlap with the postsynaptic density (PSD)-95, NMDA and AMPA receptor clusters apposed to Vglut-1-positive terminals while no colocalization of Kal7 with inhibitory presynaptic (GAD65) or postsynaptic (GABA receptors) markers was detected (32). Importantly, Kal7 expression is essential for the maintenance of dendritic spines and branching (30). Thus, a genetically mediated decrease in Kal7 expression in neuronal cultures results in loss of spines along with a reduction in dendritic length and complexity in cortical and hippocampal neurons (28,30,31,33,34). Consistently, Kal7 knockout (KO) mice exhibit a significant decrease in hippocampal spine density associated with impaired hippocampal-dependent learning and deficient long-term potentiation (LTP) (29).

Interestingly, Kal7 interacts with huntingtin-associated protein 1 (35). However, the role of Kal7 in HD pathology has not been explored. We, therefore, set out to analyze whether Kal7 plays a role in corticostriatal synaptic and cognitive deficits in HD by altering the structure and function of cortical and/or striatal excitatory synapses. Our findings show a significant and early loss of Kal7 in the cortex of HD mice associated with a decrease in dendritic spines and excitatory synapses, providing important evidence for a critical role of Kal7 in HD cortical dysfunction. Altogether, this study presents new insights for therapeutic strategies to restore early corticostriatal-dependent cognitive deficits in HD.

Results

Motor learning is impaired in HD mouse models at early disease stages

Impairment of various skill acquisition tasks involving corticostriatal circuits has been demonstrated in HD patients (36–40). Therefore, motor learning was evaluated in two different HD mouse models, mutant $Hdh^{Q7/Q111}$ knock-in mice and R6/1 mice using the accelerating rotarod task at different disease stages (11,41,42). These two HD models differ in the onset and progression of HD pathology, with R6/1 mice showing earlier onset and faster disease progression than $Hdh^{Q7/Q111}$ knock-in mice (43).

We first examined $Hdh^{Q7/Q111}$ knock-in mice (Fig. 1). At 1 month of age, motor skill acquisition did not differ between genotypes ($Hdh^{Q7/Q111}$ mice—genotype: $F_{(1,220)} = 0.8606$; $P = 0.3646$, n.s.; time: $F_{(11,220)} = 8.756$; $P < 0.0001$) (Fig. 1A). However, at 2 months of age, even though both wild-type (WT) and mutant mice learned the rotarod task ($Hdh^{Q7/Q111}$ mice—time: $F_{(11,231)} = 59.14$; $P < 0.0001$; R6/1 mice—time: $F_{(11,253)} = 11.07$; $P < 0.0001$), a significant delay in the acquisition of new motor skills was observed in $Hdh^{Q7/Q111}$ mice ($Hdh^{Q7/Q111}$ mice—genotype: $F_{(1,231)} = 13.30$; $P = 0.0015$) (Fig. 1B). Importantly, at 6 and 8 months of age, $Hdh^{Q7/Q111}$ mice were unable to maintain the balance on the rotarod and showed a significant and progressive decrease in the latency to fall (genotype: $F_{(1,209)} = 27.77$; $P < 0.0001$; time: $F_{(11,209)} = 27.24$; $P < 0.0001$) (Fig. 1C and D). Altogether, these findings demonstrate an age-dependent impairment of motor learning in $Hdh^{Q7/Q111}$ mice. Because poor performance in the accelerating rotarod at advanced disease stages could be due to motor coordination deficits, performance on the fixed rotarod was analyzed in $Hdh^{Q7/Q111}$ knock-in mice at 2, 6 and 8 months of age. Although 2- and 6-month-old $Hdh^{Q7/Q111}$ knock-in mice were able to appropriately perform the fixed rotarod task (Fig. 1E and F), at 8 months of age, motor coordination was severely impaired, showing $Hdh^{Q7/Q111}$ knock-in mice a significant increase in the number of falls compared with WT $Hdh^{Q7/Q7}$ mice (Fig. 1G). Similar results were found when spontaneous locomotor activity was measured in the open field with no differences in the distance traveled by $Hdh^{Q7/Q111}$ knock-in mice compared with WT $Hdh^{Q7/Q7}$ mice at 2 and 6 months of age but a deficit at 8 months of age (Supplementary Material, Fig. S1).

Comparable data were obtained when R6/1 mice were analyzed (Fig. 2). No differences in the motor skill acquisition were detected between WT and R6/1 mice at 1 month of age (genotype: $F_{(1,264)} = 0.03423$; $P = 0.8548$, n.s.; time: $F_{(11,264)} = 7.391$; $P < 0.0001$) (Fig. 2A). However, at 2 months of age, R6/1 mice were unable to maintain the balance on the rotarod and showed significantly lower latency to fall compared with WT mice (R6/1 mice—genotype: $F_{(1,253)} = 7.831$; $P = 0.0102$) (Fig. 2B). Importantly, this impairment in the acquisition of new motor skills worsened along the disease progression evidenced by a significant decrease in the latency to fall from the rotarod at 3 months of age (genotype: $F_{(1,242)} = 11.78$; $P = 0.0024$; time: $F_{(11,242)} = 16.84$; $P < 0.0001$) (Fig. 2C). It is important to notice that R6/1 mice do not exhibit motor impairments in the fixed rotarod until 3 months of age (44). Thus, altogether these data demonstrate that at early and mild disease stages, both knock-in and R6/1 mice show motor learning deficits without motor coordination alterations, whereas at more advanced disease stages, cognitive deficits were accompanied by motor coordination dysfunction.

HD mice exhibit procedural memory deficits in a Swimming T-maze test

Learning deficits were validated in HD mice by analysis of procedural memory in the Swimming T-maze test. The task was performed in 6-month-old $Hdh^{Q7/Q111}$ (Fig. 3A–D) and 2-month-old R6/1 (Fig. 3E–H) mice, because at these ages, we have shown motor learning deficits without motor coordination impairments. During the acquisition phase, the escape platform was located in the right arm of the T-maze and the latency to reach the platform and the number of ‘errant’ trials (turning left to reach

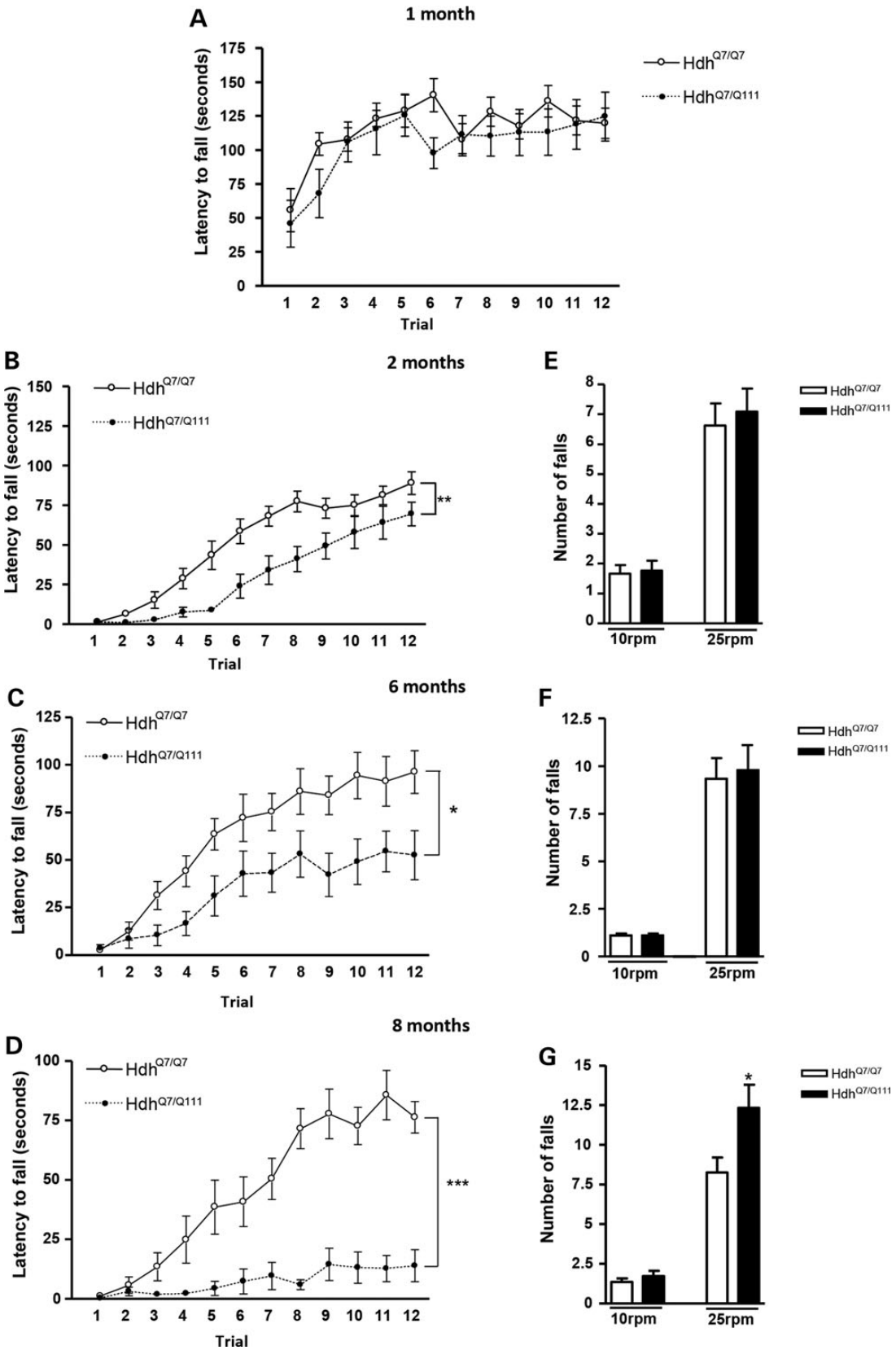

Figure 1. $Hdh^{Q7/Q111}$ knock-in mutant mice display impaired learning of new motor skills at early disease stages when no motor coordination deficits are observed. Latency to fall in the accelerating rotarod task for WT $Hdh^{Q7/Q7}$ and knock-in $Hdh^{Q7/Q111}$ mutant mice at 1 (**A**), 2 (**B**), 6 (**C**) and 8 (**D**) months of age. An age-dependent impairment in motor learning was observed in HD mice. Data represent the mean ± SEM (n = 9–14 per genotype). Statistical analysis was performed using two-way ANOVA with repeated measures. *$P < 0.05$; **$P < 0.01$; ***$P < 0.001$. Number of falls in the fixed rotarod at 10 and 25 rpm in WT $Hdh^{Q7/Q7}$ and knock-in $Hdh^{Q7/Q111}$ mutant mice at 2 (**E**), 6 (**F**) and 8 (**G**) months of age. No motor coordination deficits were observed until 8 months of age in $Hdh^{Q7/Q111}$ mice. Data represent the mean ± SEM (n = 9–15 per genotype). Statistical analysis was performed using one-way ANOVA with *post hoc* Bonferroni's multiple comparison test. *$P < 0.05$.

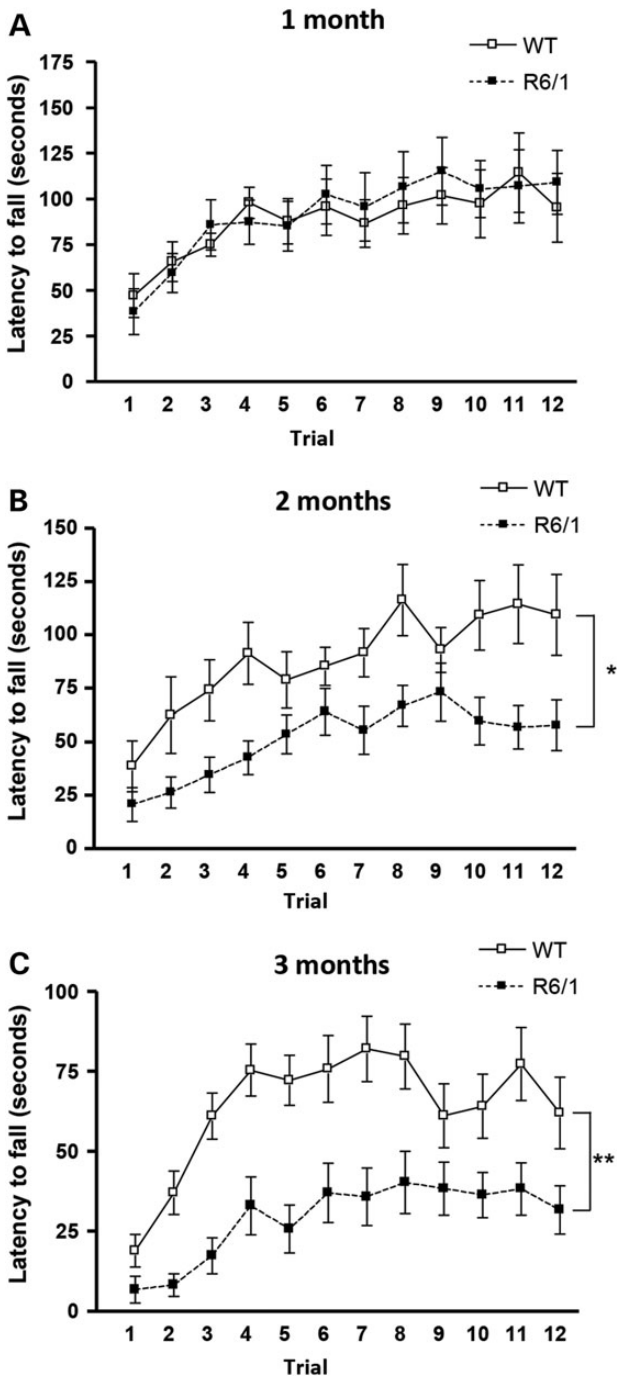

Figure 2. R6/1 mice exhibit impaired learning of new motor skills at early disease stages. Latency to fall in the accelerating rotarod task for WT and R6/1 mice at 1 (**A**), 2 (**B**) and 3 (**C**) months of age. An age-dependent impairment in motor learning was observed in R6/1 mice. Data represent the mean ± SEM ($n = 9$–14 per genotype). Statistical analysis was performed using two-way ANOVA with repeated measures. *$P < 0.05$; **$P < 0.01$.

the platform) was scored. After one trial, both WT and HD mice exhibited a similar decrease in the latency to reach the platform, showing by the last trial, a constant level of performance (~10 s to reach the platform; Fig. 3A and E). However, when the number of errant trials was analyzed, HD mice showed a trend increase, although no significant, in the error probability compared with WT mice (Fig. 3C and G). Interestingly, this difference in the number of errant trials was normalized in the last trial, indicating that HD mice present a delay but not impairment in the acquisition of this task.

Next, the ability of HD mice to change the strategy was assessed by switching the platform from the right arm to the left arm of the T-maze (reversal phase). Contrary to what was observed during the acquisition phase, the latency to reach the platform was now significantly higher in HD mice compared with WT mice (Fig. 3B and F). This increase was likely related with the higher number of errant trials exhibited by HD mice. Thus, in WT mice, the error ratio by the fourth trial was 0.5, meaning that approximately half turned right and half turned left, whereas in HD mice, it was ~0.8, indicating that most of the HD mice entered the right arm (Fig. 3D and H). Overall, these results demonstrate that both knock-in and R6/1 mice exhibit changing strategy problems evidenced by an increase in the latency to reach the platform and the error ratio in the reversal phase of the Swimming T-maze test.

Functional and structural synaptic plasticity is altered in Hdh$^{Q7/Q111}$ knock-in mice

Altered synaptic transmission and plasticity may contribute to behavioral deficits in HD mice (1,2). Therefore, we next addressed whether impaired motor learning in HD mice was related to dysfunctional corticostriatal synaptic plasticity. Because 8- to 10-week-old R6/1 mice are known to display deficits in cortical synaptic plasticity (2), electrophysiological studies were only conducted in WT Hdh$^{Q7/Q7}$ and mutant Hdh$^{Q7/Q111}$ knock-in mice. Synaptic potentials were evoked by stimulation of corticostriatal glutamatergic fibers in slices obtained from mutant Hdh$^{Q7/Q111}$ and WT Hdh$^{Q7/Q7}$ mice at 2–3 months of age (Fig. 4A). Baseline responses were monitored for 10–30 min before conditioning and were found to be stable. Tetanus conditioning revealed a marked difference in the ability of mutant Hdh$^{Q7/Q111}$ mice to support corticostriatal LTP with strengthening of population spike (PS) significantly diminished in mutant mice (Fig. 4A, $P < 0.001$). Thus, at 60 min after tetanus, potentiation in WT Hdh$^{Q7/Q7}$ mice was 133 ± 3% ($n = 7$ slices; three mice) versus 104 ± 3% in mutant Hdh$^{Q7/Q111}$ knock-in mice ($n = 8$ slices; three mice), which indicates impaired induction and maintenance of corticostriatal LTP in mutant Hdh$^{Q7/Q111}$ knock-in mice.

Next, we explored whether the observed corticostriatal LTP deficits could be related with structural synaptic changes in the cortex and/or striatum of Hdh$^{Q7/Q111}$ mice. To this aim, dendritic spine density was analyzed in fixed brain slices containing both cortex and striatum obtained from 2-month-old Hdh$^{Q7/Q7}$ and Hdh$^{Q7/Q111}$ mice by using DiOlistic labeling (Fig. 4B). Confocal stacks z-projections from segments of apical dendrites of motor cortical (M1) and medium spiny striatal neurons were used for the quantitative analyses of dendritic spines. The number of spines per micrometer of dendrite length was significantly reduced (~10%; $P < 0.01$) in the motor cortex of Hdh$^{Q7/Q111}$ knock-in mice compared with Hdh$^{Q7/Q7}$ WT mice. Importantly, no significant differences were detected between genotypes when the number of dendritic spines was analyzed in the medium spiny neurons within the dorsal striatum.

To elucidate whether spine morphology was also affected in 2-month-old Hdh$^{Q7/Q111}$ mice, the type of dendritic spines (mushroom, thin or stubby) was analyzed (Fig. 4B). Higher proportion of thin spines compared with mushroom spines was observed in WT cortical neurons, whereas a similar proportion was found in mutant cortical neurons. As for dendritic spine density, no changes on spine-type distribution were found in medium

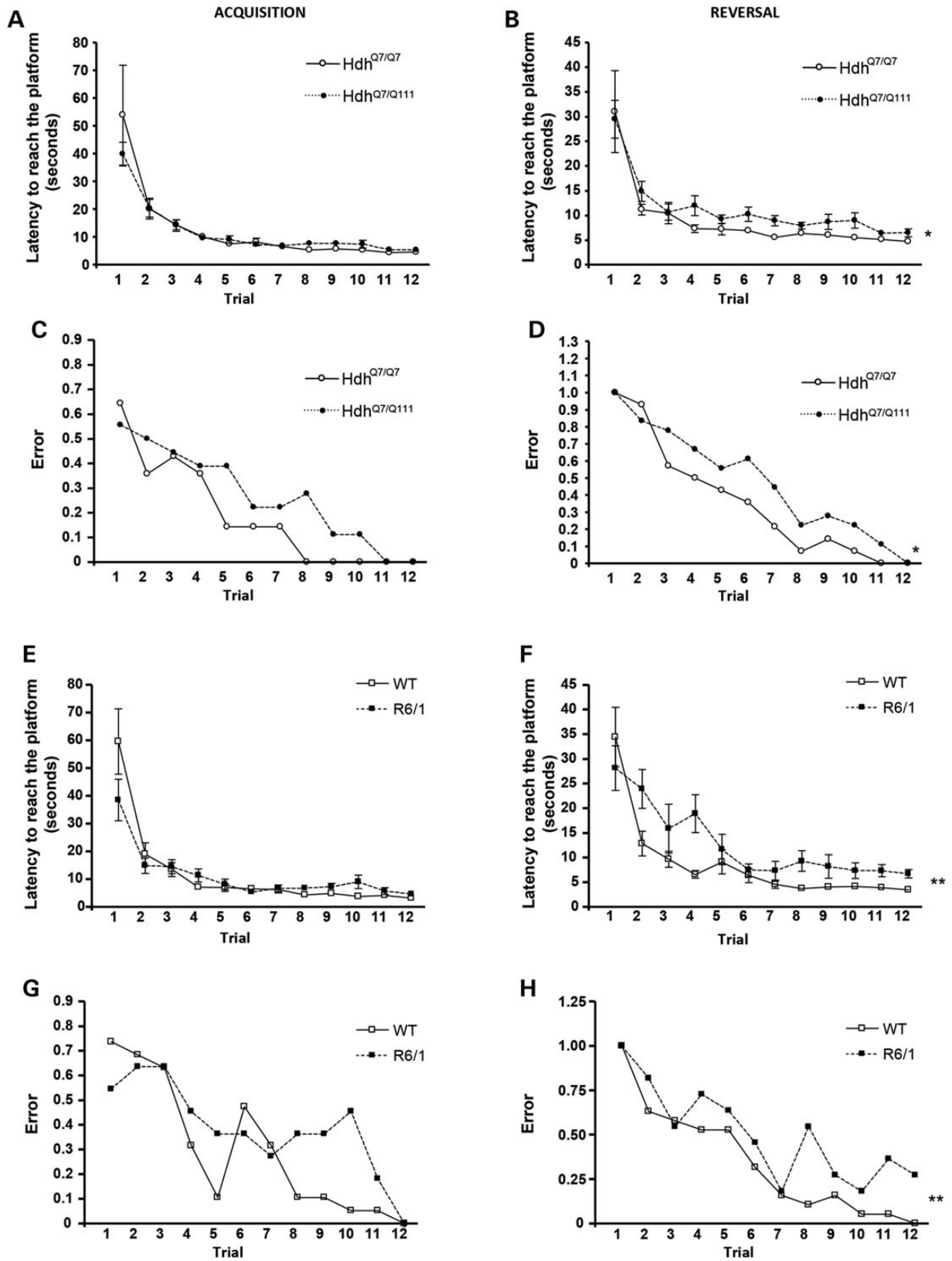

Figure 3. $Hdh^{Q7/Q111}$ and R6/1 mice display early impairments in procedural memory. Latency to reach the platform and error trials in the Swimming T-maze test in 6-month-old WT $Hdh^{Q7/Q7}$ and knock-in $Hdh^{Q7/Q111}$ mice and in 2-month-old WT and R6/1 mice during the acquisition (**A**, **C**, **E** and **G**) and reversal (**B**, **D**, **F** and **H**) phases of the Swimming T-maze test of strategy shifting. HD mice exhibited procedural memory deficits in the reversal phase of the Swimming T-maze test. Data represent the mean ± SEM ($n = 11–19$ per genotype). Statistical analysis was performed using two-way ANOVA with repeated measures to analyze the latency to reach the platform: $^{*}P < 0.05$; $^{**}P < 0.01$. Logistic regression analysis using the Wald statistical test from IBM SPSS Statistics was used to analyze the error probability to reach the platform in the correct arm: $^{*}P < 0.05$; $^{**}P < 0.01$.

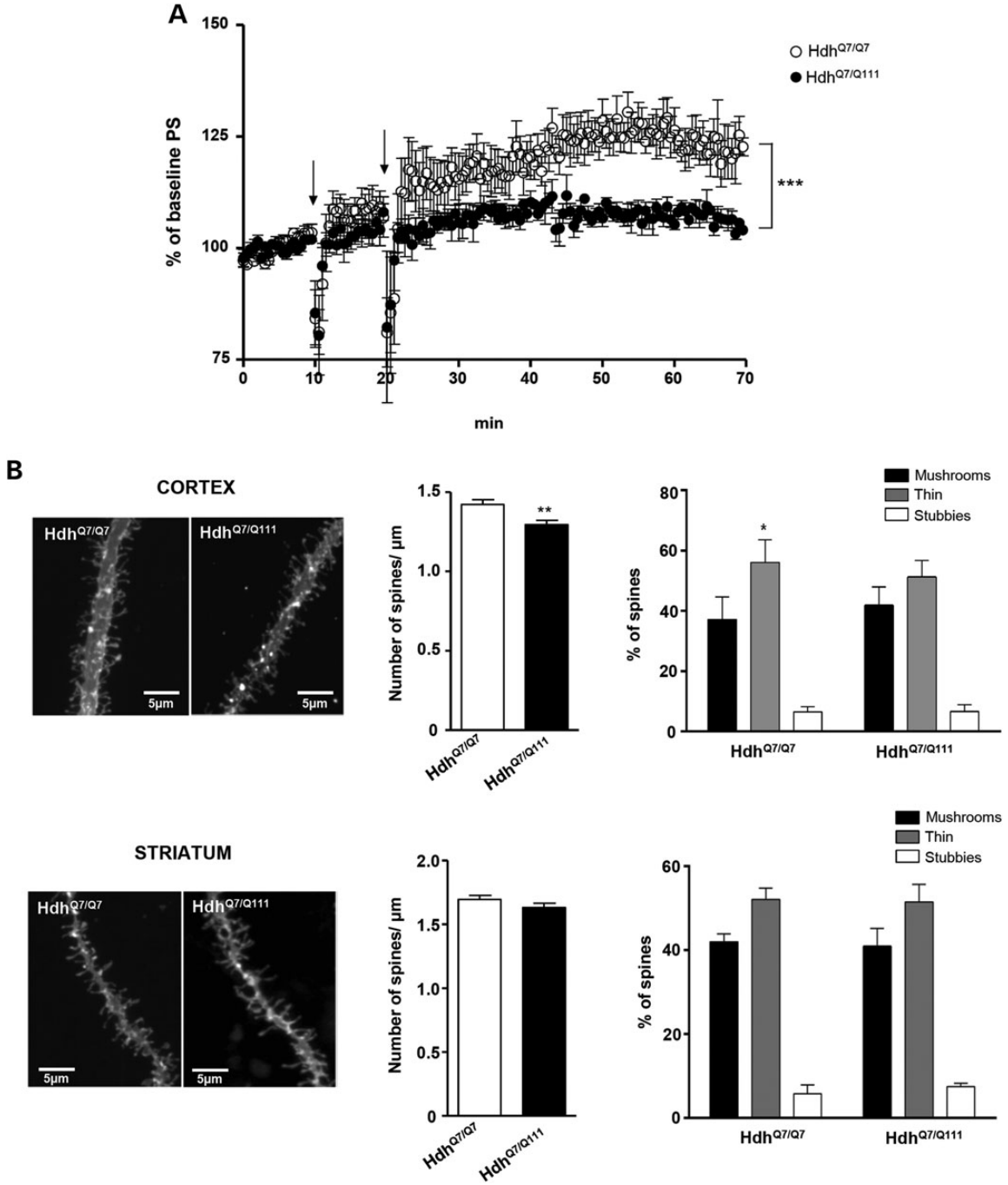

Figure 4. Abnormal corticostriatal synaptic plasticity and altered cortical dendritic spines in $Hdh^{Q7/Q111}$ mice at 2 months of age. (**A**) Summary data showing the time course of mean PS slope in WT $Hdh^{Q7/Q7}$ (open circle, $n = 7$) and knock-in mutant $Hdh^{Q7/Q111}$ (filled circle, $n = 8$) mice at 2–3 months of age in basal conditions and following LTP induction (arrows). For each slice, data were normalized to the average slope recorded during baseline. Data represent the mean ± SEM. Statistical differences, compared with pre-tetanus baseline amplitude values, were established using Student's two-tailed *t* test. ***$P < 0.001$. (**B**) (Left) Representative apical dendrites of the cortical pyramidal neurons of the motor cortex and dendrites of striatal medium spiny neurons of dorsal striatum from WT $Hdh^{Q7/Q7}$ and knock-in mutant $Hdh^{Q7/Q111}$ mice. Quantitative analysis showing dendritic spine density per micrometer of dendritic length. Knock-in $Hdh^{Q7/Q111}$ mice exhibit a significant reduction in cortical but not striatal dendritic spines. One-way ANOVA with Tukey *post hoc* comparisons was performed (63–83 dendrites; $n = 4$ animals per genotype); **$P < 0.01$ compared with $Hdh^{Q7/Q7}$ mice. (Right) Percentage of each morphological type of dendritic spine (see Materials and Methods for classification criteria) from WT $Hdh^{Q7/Q7}$ and knock-in mutant $Hdh^{Q7/Q111}$ mice at 2 months of age. One-way ANOVA with Tukey *post hoc* comparisons was performed (cortex: 319 spines from 30 dendrites from 4 animals per genotype; striatum: 280 spines from 25 dendrites from 4 animals per genotype were analyzed); *$P < 0.01$ (mushrooms versus thin spines).

spiny striatal neurons. Altogether, these findings show a specific and early alteration of dendritic spines in the motor cortex of $Hdh^{Q7/Q111}$ mice in the absence of prominent structural synaptic changes in the striatum.

Spinophilin-immunoreactive puncta are reduced in the cortex but not in the striatum of $Hdh^{Q7/Q111}$ knock-in mice

To analyze structural synaptic alterations in $Hdh^{Q7/Q111}$ mice in the early and late stages of disease progression, spinophilin

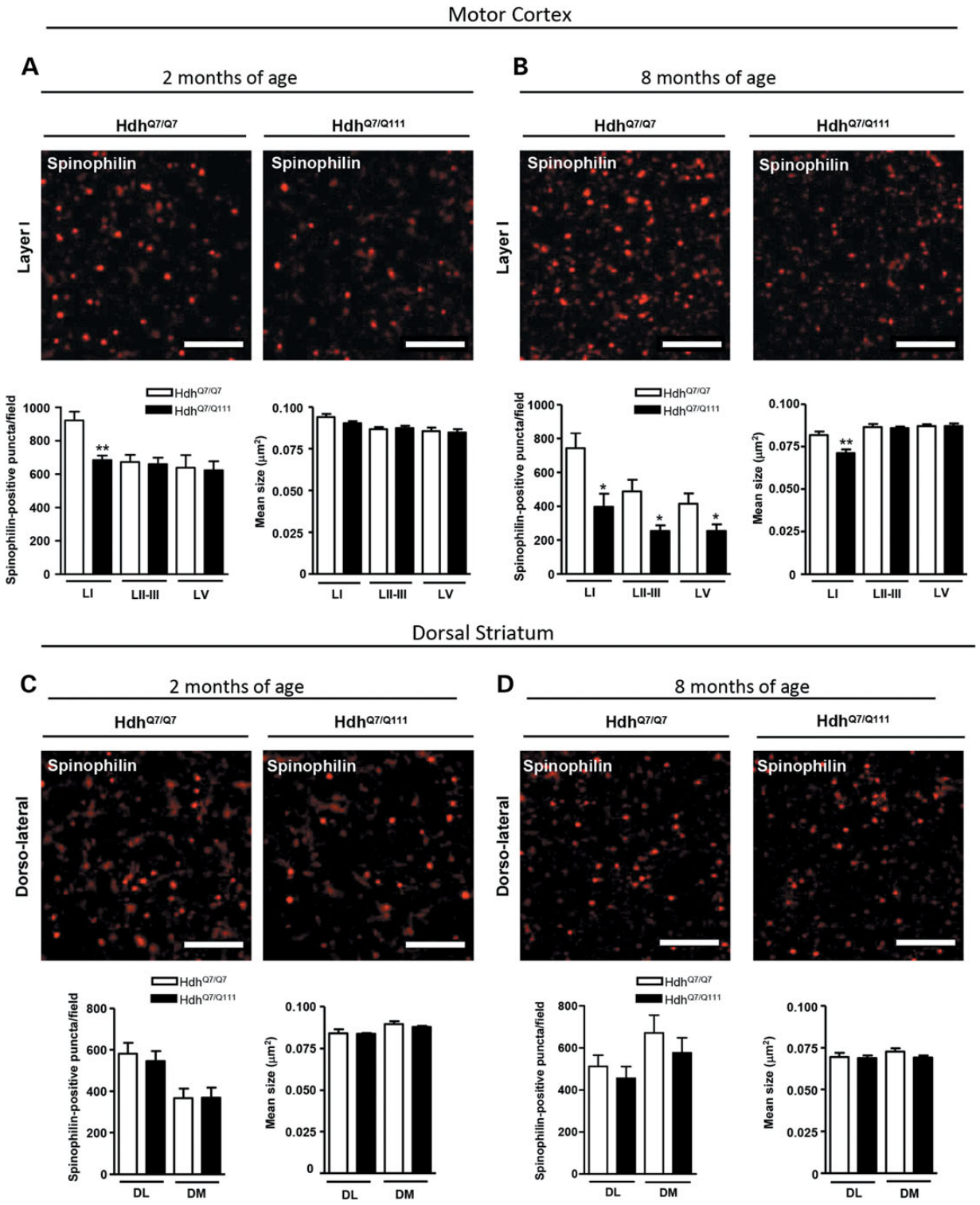

Figure 5. Spinophilin-immunoreactive puncta are reduced in the motor cortex but not in the striatum of Hdh$^{Q7/Q111}$ mice. Representative confocal images showing spinophilin (red) positive clusters in the motor cortex (**A** and **B**) and dorsal striatum (**C** and **D**) of WT Hdh$^{Q7/Q7}$ and knock-in Hdh$^{Q7/Q111}$ mice at 2 (A and C) and 8 (B and D) months of age. Spinophilin-immunoreactive puncta were counted and mean size evaluated in layers I, II/III and V of motor cortex area 1 (M1) and in the DL and DM striatum. Quantitative analysis is shown as mean ± SEM ($n = 5$–6 animals per group). A specific reduction in spinophilin-immunoreactive puncta was found in the cortex but not in the striatum of knock-in Hdh$^{Q7/Q111}$ mice from early disease stages. Statistical analysis was performed using Student's two-tailed t test. $^{*}P < 0.05$; $^{**}P < 0.01$ compared with Hdh$^{Q7/Q7}$ mice. Scale bar, 5 µm.

immunostaining was performed in cortical (motor cortex) and striatal (dorsal striatum) slices obtained from WT Hdh$^{Q7/Q7}$ and mutant Hdh$^{Q7/Q111}$ knock-in mice at 2 and 8 months of age (Fig. 5). Spinophilin is a protein phosphatase 1-binding protein localized primarily in dendritic spines (45,46), where it labels 90% of spines (47,48), with some marginal labeling of dendrites

and glia (46). Confocal microscopy analysis revealed a significant reduction ($P < 0.01$) in spinophilin-immunoreactive puncta in layer I of the motor cortex of 2-month-old $Hdh^{Q7/Q111}$ mice compared with WT $Hdh^{Q7/Q7}$ mice (Fig. 5A) without significant changes in the striatum (Fig. 5C). Interestingly, at 8 months of age, the decrease in spinophilin-immunoreactive puncta in motor cortex layer I was more pronounced ($P < 0.05$) than the decrease observed at 2 months of age and was accompanied by a decrease in layers II–III and V ($P < 0.05$) (Fig. 5B). Notice that at 8 months of age, the mean size of spinophilin puncta was also reduced in motor cortex layer I ($P < 0.01$) (Fig. 5B). Notably, spinophilin immunoreactivity was not affected in the striatum of mutant $Hdh^{Q7/Q111}$ mice either at 2 months or at 8 months of age (Fig. 5D), further supporting the idea that in HD knock-in mice, cortical structural changes may precede those in the striatum.

PSD-95-positive puncta are decreased in the cortex but not in the striatum of $Hdh^{Q7/Q111}$ knock-in mice at early disease stages

Because most excitatory synapses in the mammalian brain are formed on dendritic spines (49) and HD knock-in mice have demonstrated decreased structural plasticity in the cortex, we next asked whether excitatory postsynaptic sites were also altered in the cortex and/or striatum of $Hdh^{Q7/Q111}$ knock-in mutant mice. To this aim, PSD-95 immunoreactive puncta was analyzed in the motor cortex and dorsal striatum of WT $Hdh^{Q7/Q7}$ and mutant $Hdh^{Q7/Q111}$ knock-in mice at 2 and 8 months of age. A significant reduction in the number of PSD-95-immunoreactive puncta was found in motor cortex layer I ($P < 0.01$) and layers II–III ($P < 0.05$) of 2-month-old mutant $Hdh^{Q7/Q111}$ knock-in mice compared with WT $Hdh^{Q7/Q7}$ mice along with a decrease in the mean size of PSD-95 clusters in layer I (Fig. 6A). Importantly, at this age, no significant changes were found in the dorsal striatum of mutant $Hdh^{Q7/Q111}$ mice either in the number or in size of PSD-95-immunoreactive puncta (Fig. 6C).

Conversely, analysis of PSD-95 immunostaining at 8 months of age revealed a drastic reduction in the number and size of PSD-95-immunoreactive puncta in all the cortical layers analyzed (Fig. 6B; $P < 0.05$ and 0.01) along with a significant decline (Fig. 6D; $P < 0.05$ and 0.01) in the number of PSD-95 clusters in the dorsal striatum of $Hdh^{Q7/Q111}$ mutant mice compared with WT $Hdh^{Q7/Q7}$ mice. These data reveal an early decrease of glutamatergic excitatory postsynaptic sites in the cortex of mutant $Hdh^{Q7/Q111}$ knock-in mice, worsening thereafter and involving, at later disease stages, the striatum.

Cortical structural changes in young $Hdh^{Q7/Q111}$ knock-in mice correlate with reduced levels of the Rho-GEF protein Kal7

The structural alterations demonstrated in the cortex of mutant $Hdh^{Q7/Q111}$ knock-in mice at early disease stages prompted us to investigate by western blot the levels of distinct pre- and postsynaptic proteins in total cortical and striatal extracts obtained from WT $Hdh^{Q7/Q7}$ and knock-in $Hdh^{Q7/Q111}$ mutant mice at 2 and 8 months of age. First, we analyzed the levels of the postsynaptic proteins spinophilin and PSD-95. Similar levels of both proteins were found between WT and mutant mice either in the cortex or in the striatum at 2 months of age (Fig. 7A and B). Similarly, when other PSD components such as the glutamate receptors GluA1 (AMPA receptor subunit), GluN1 and GluN2B (NMDA receptor subunits) or the postsynaptic scaffolding protein Shank3 were analyzed, no differences between genotypes were found (Fig. 7A and B). Next, the levels of two important signaling molecules, CaMKII and the brain-specific Rho-GEF protein Kal7, were analyzed. No changes in the levels of CaMKII were found between genotypes. In contrast, Kal7 levels were found to be significantly reduced in the cortex but not in the striatum of $Hdh^{Q7/Q111}$ mutant mice when compared with WT $Hdh^{Q7/Q7}$ mice ($P < 0.05$; Fig. 7A and B). It is important to notice that no differences in the levels of the presynaptic proteins Vglut1 and Synaptophysin were observed between genotypes, neither in the cortex nor in the striatum. Altogether, these results suggest that the structural plasticity changes found in the cortex of young $Hdh^{Q7/Q111}$ mutant mice could be associated with a specific decrease of Kal7 levels rather than with a general reduction in PSD-associated proteins or in presynaptic markers.

Next, the levels of all these synaptic-related proteins were analyzed at 8 months of age. At this age, the decrease in Kal7 levels was accompanied by a significant reduction in cortical PSD-95 ($P < 0.05$) and Shank3 ($P < 0.05$) levels and by a decrease in the levels of striatal PSD-95 ($P < 0.05$) (Fig. 7A and B). These data suggest that at more advanced HD stages, both structural and biochemical changes in the cortex and striatum could contribute to corticostriatal pathology in HD.

Kal7 levels are reduced in R6/1 mutant transgenic mice and in HD human brain

To determine whether the decrease in Kal7 levels is a general hallmark of HD pathology, the levels of Kal7 were also determined in the cortex and striatum of R6/1 transgenic mice (Fig. 8A). Consistent with our previous data, Kal7 levels were found to be significantly reduced in the cortex but not in the striatum of R6/1 mice at 2 ($P < 0.01$) and 3 ($P < 0.001$) months of age, without any significant decrease in other synaptic-related proteins, with the exception of Vglut1 and CamKII, respectively (Supplementary Material, Fig. S2).

Next, we investigated the levels of Kal7 in postmortem brain tissue from the cortex and putamen of control and HD individuals. Quantitative immunoblot analysis revealed a significant decrease of Kal7 levels not only in the cerebral cortex (control: 100 ± 6.702, HD: 52.75 ± 5.851; $P = 0.0008$) but also in the putamen (control: 100 ± 15.38, HD: 29.46 ± 7.383; $P = 0.0033$) of HD patients compared with controls (Fig. 8B). However, data in human samples may indicate a general process of cell death or neuronal atrophy. To determine the specificity of Kal7 reduction in HD brain, levels of glutamate receptor units GluN1 and GluA1, shown to be not altered in HD mice, were analyzed. No significant differences between HD and control brain samples were found, suggesting a selective decrease of Kal7 in human HD cortex. In contrast, HD putamen samples exhibited, along with altered Kal7 levels, a significant decrease in GluN1 (control: 100 ± 6.166, HD: 65.67 ± 13.14; $P = 0.0396$) likely related with the severe striatal neuronal death characteristic of HD human brain (50,51).

Altogether, these results showing specific cortical reduction of Kal7 levels in both HD mice and HD patients suggest an important role for Kal7 in HD pathology.

The activity of the Rho-GTPase Rac1 is decreased in the cortex of $Hdh^{Q7/Q111}$ knock-in mutant mice

Activation of Rac1 mediated by Kal7 is critical for the regulation of activity-dependent changes in spine morphology and plasticity (26,52). Given the reduction of Kal7 levels in the cortex of HD mice, we investigated whether such decrease was associated with diminished activity of the small GTPase Rac1. Pull-down

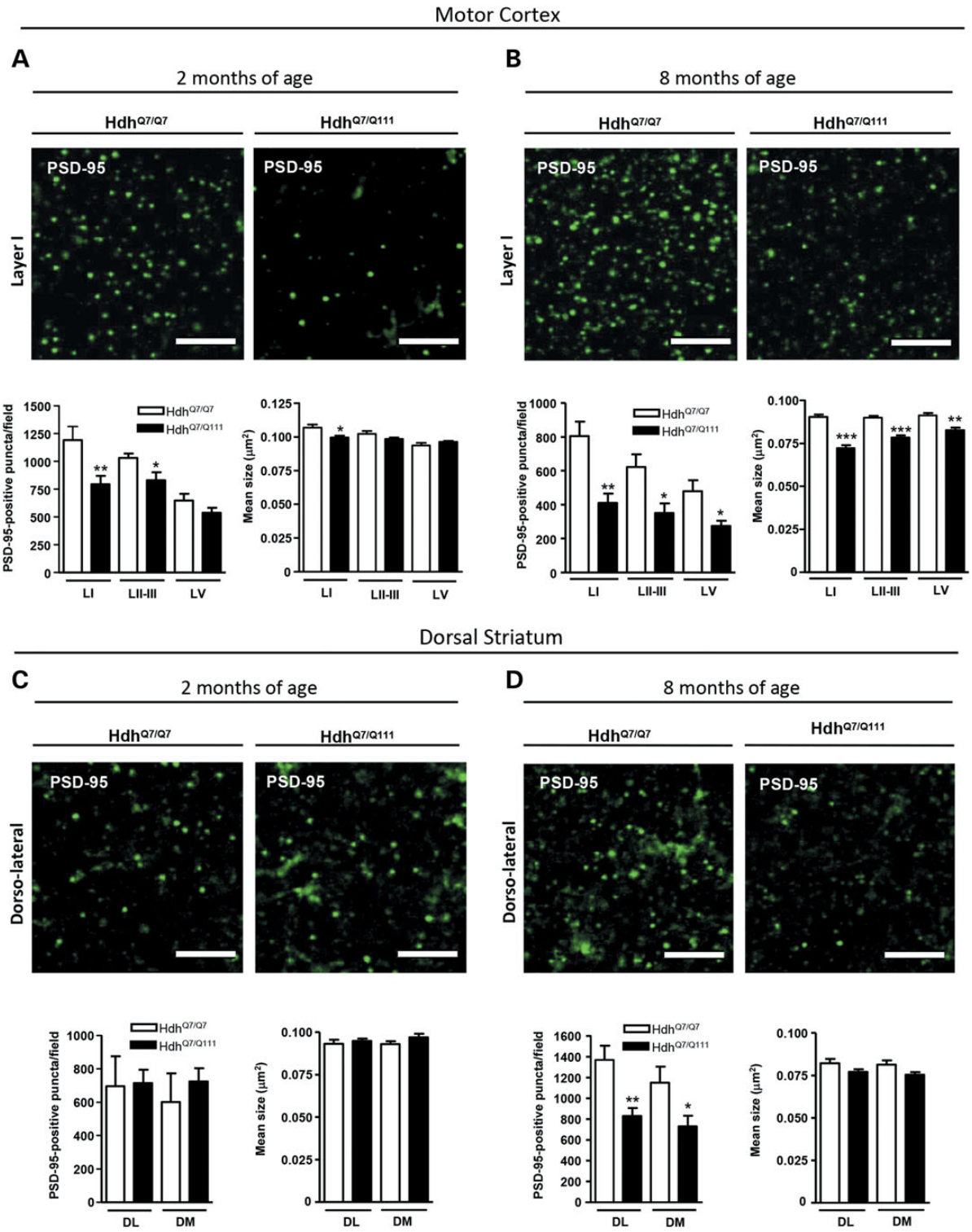

Figure 6. PSD-95-immunoreactive puncta are decreased at early disease stages in the motor cortex of $Hdh^{Q7/Q111}$ mice. Representative confocal images showing PSD-95 (green) positive clusters in the motor cortex (**A** and **B**) and dorsal striatum (**C** and **D**) of WT $Hdh^{Q7/Q7}$ and mutant knock-in $Hdh^{Q7/Q111}$ mice at 2 (A and C) and 8 (B and D) months of age. Cortical PSD-95-immunoreactive puncta were counted and mean size evaluated in layers I, II/III and V of motor cortex area 1 (M1) and in the DL and DM striatum. Quantitative analysis is shown as mean ± SEM ($n = 5$–6 animals per group). A specific reduction in PSD-95-immunoreactive puncta was found in cortex but not striatum of $Hdh^{Q7/Q111}$ mice at early disease stages. At more advanced disease stages, a reduction in PSD-95-immunoreactive puncta was also found in the dorsal striatum. Statistical analysis was performed using Student's two-tailed *t* test. $^{*}P < 0.05$; $^{**}P < 0.01$; $^{***}P < 0.001$ compared with $Hdh^{Q7/Q7}$ mice. Scale bar, 5 µm.

assays on cortical extracts obtained from WT $Hdh^{Q7/Q7}$ and mutant $Hdh^{Q7/Q111}$ knock-in mice revealed a significant decrease in Rac1 activation evidenced by a decrease in the levels of Rac1-GTP in mutant compared with WT mice ($Hdh^{Q7/Q7}$: 100 ± 15.5%, $Hdh^{Q7/Q111}$: 48.0 ± 13.0%, $P < 0.05$). Notice that total Rac1 levels were similar between both genotypes ($Hdh^{Q7/Q7}$: 100 ± 15.2%,

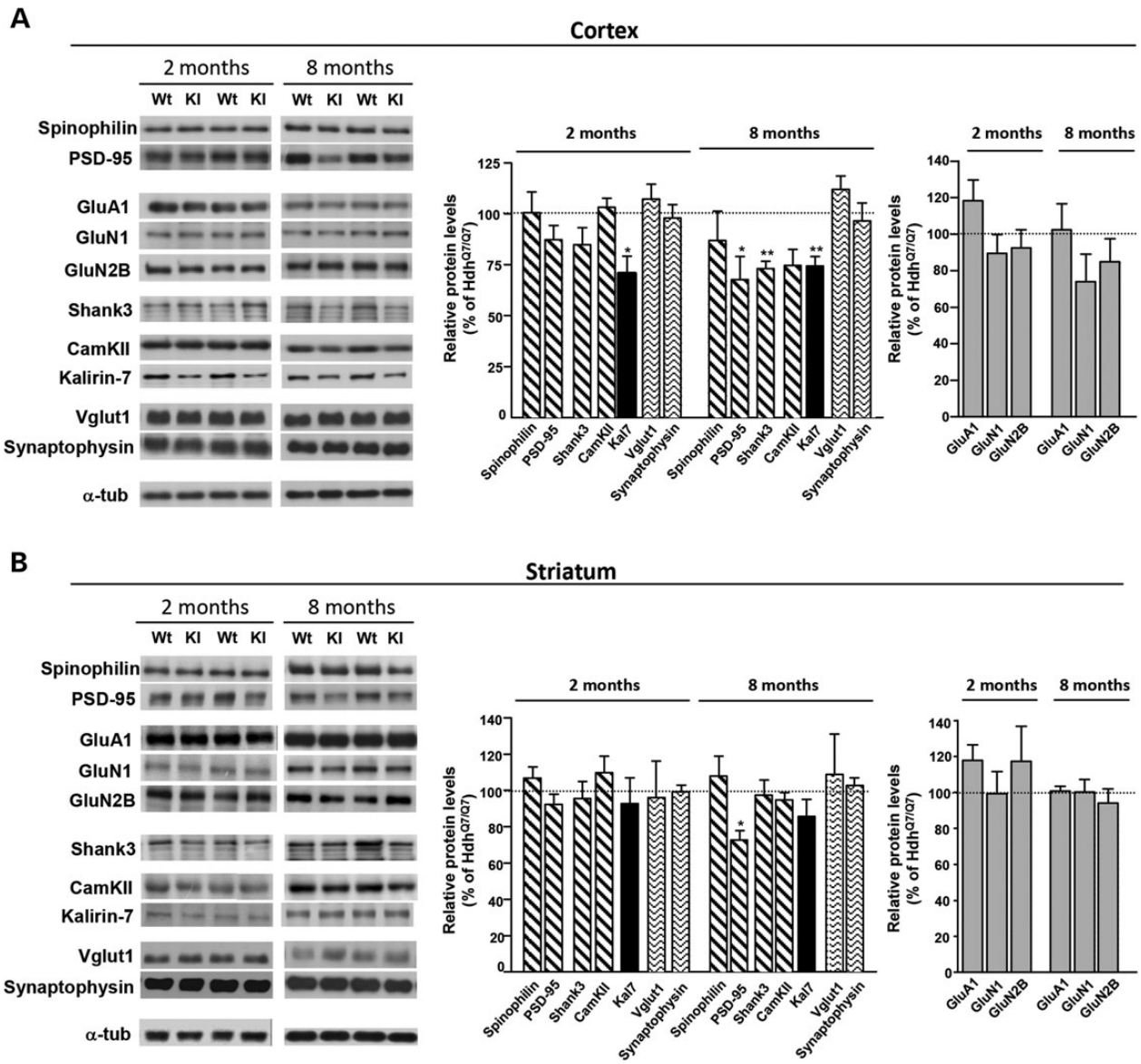

Figure 7. Levels of Kal7 are reduced in the cortex but not in the striatum of $Hdh^{Q7/Q111}$ mice at early disease stages. Representative western blots showing the indicated subunits of glutamate receptors, pre- and postsynaptic scaffolding proteins and protein kinases in the total cortical (**A**) and striatal (**B**) extracts from 2- and 8-month-old WT $Hdh^{Q7/Q7}$ and knock-in $Hdh^{Q7/Q111}$ mutant mice. α-Tubulin was used as a loading control. A specific reduction in Kal7 was found in the cortex but not in the striatum of $Hdh^{Q7/Q111}$ mutant mice compared with $Hdh^{Q7/Q7}$ WT mice at 2 months of age. At more advanced disease stages, a reduction in other synaptic-related proteins was found. Histograms represent the mean ± SEM and are expressed as percentage of WT animals ($n = 5–8$ animals per genotype). Statistical analysis was performed using Student's two-tailed t test. $^*P < 0.05$; $^{**}P < 0.01$ compared with $Hdh^{Q7/Q7}$ mice.

$Hdh^{Q7/Q111}$: 98.4 ± 1 6.5%, $P = 0.9462$) (Fig. 9). These results suggest that decreased GTPase Rac1 activity due to reduced Kal7 levels could contribute to corticostriatal dysfunction in HD mice.

Maintenance of excitatory synapses is compromised in R6/1 cortical cultures

Our previous findings showing reduced Kal7 levels and Rac1 activity in the cortex of HD mice suggest that deficient Kal7 function could contribute to early cortical structural changes in HD mice. To explore this hypothesis, we wondered whether these deficits could also be reproduced *in vitro*. To this aim, the pattern of Kal7 expression was determined by western blot analysis in WT cortical cultures at different days *in vitro* (DIV). Expression of Kal7 was not detectable until DIV14 remaining stable by DIV21 and DIV28 and similar to adult brain levels (Supplementary Material, Fig. S3). Next, levels of Kal7 were compared between WT and R6/1 cortical cultures both at DIV14 and DIV28. Similar to our *in vivo* data, Kal7 levels were significantly reduced (~25%; $P < 0.05$) in R6/1 compared with WT cortical cultures both at DIV14 and DIV28 conditions (Fig. 10A). As we can reproduce the reduction of Kal7 levels *in vitro* and Kal7 is important for excitatory synapses, the number of Vglut1 and PSD-95-positive coclusters, as a measure of glutamatergic excitatory synapses, was determined in WT and HD mutant cortical cultures at DIV14 and DIV28. Although similar PSD-95, Vglut1 and PSD-95/Vglut1 positive clusters were found in R6/1 cortical neurons when compared with WT neurons at DIV14 (Fig. 10B), a significant decrease was detected at DIV28 (Fig. 10C), suggesting that excitatory synapses in HD mutant neurons developed normally for 14 days but then

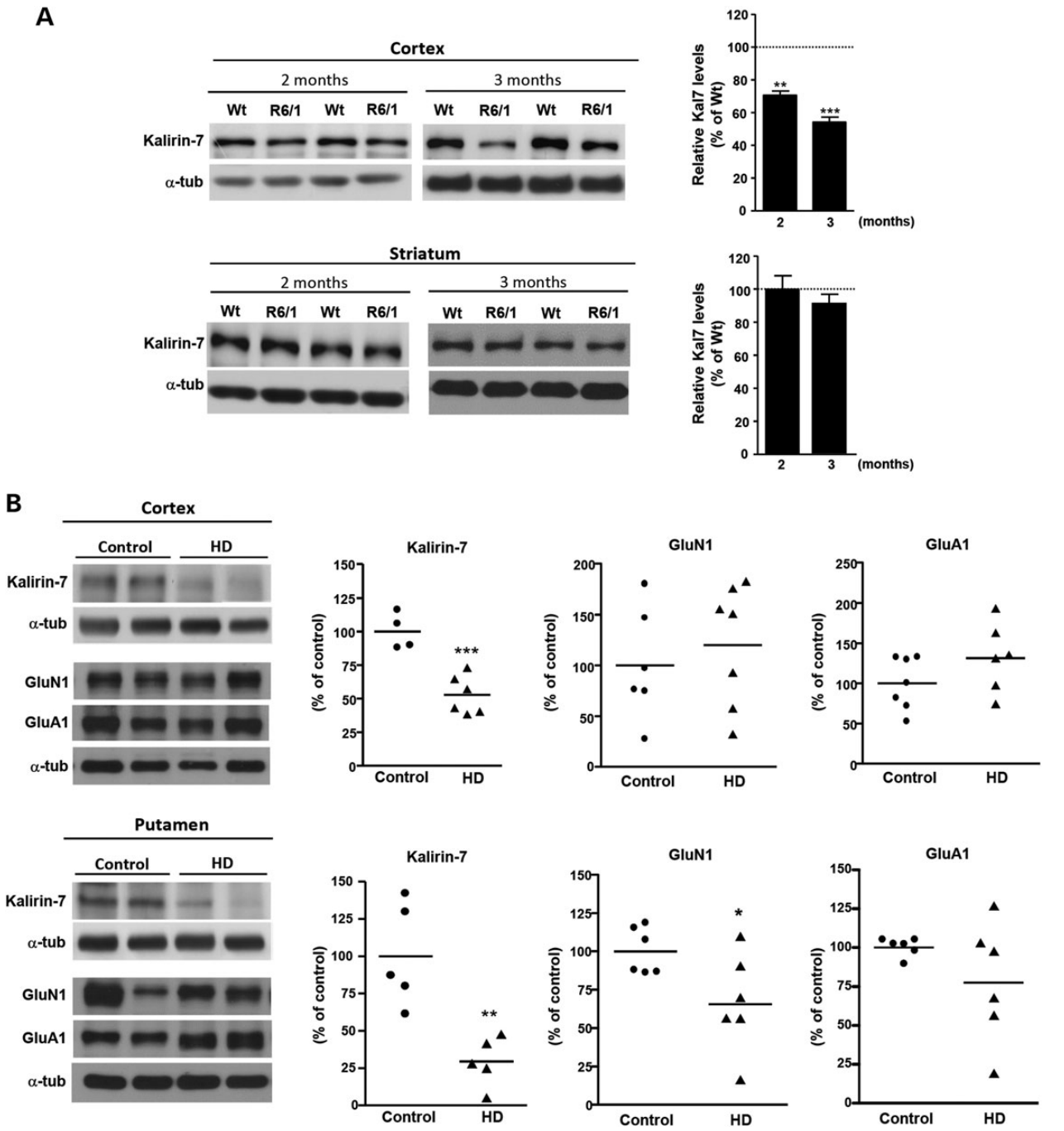

Figure 8. Kal7 levels are reduced in the cortex of R6/1 mice and in the cortex and putamen of HD brains. (**A**) Representative western blots showing Kal7 and α-tubulin as a loading control in total cortical and striatal extracts from 2- and 3-month-old WT and R6/1 mice. Histograms represent the mean ± SEM ($n = 5–8$ animals per genotype). Statistical analysis was performed using Student's two-tailed *t* test. $^{**}P < 0.01$; $^{***}P < 0.001$ compared with $Hdh^{Q7/Q7}$ mice. (**B**) Representative western blots showing Kal7, GluN1, GluA1 and α-tubulin as a loading control in total cortical and putamen extracts from control ($n = 4–7$) and HD samples ($n = 5–7$). Histograms represent mean ± SEM and are expressed as percentage of control samples. Student's two-tailed *t* test was performed. $^{*}P < 0.05$; $^{**}P < 0.01$; $^{***}P < 0.001$ compared with control human samples.

were lost by DIV28, in accordance with a role of Kal7 in the maintenance of dendritic spines (29,32).

Overexpression of exogenous Kal7 restores the number of excitatory synapses in R6/1 cortical cultures

To validate a role for Kal7 in the loss of excitatory synapses in mutant huntingtin conditions, exogenous Kal7 was overexpressed at DIV12 in WT and R6/1 cortical neurons and the number of excitatory synapses evaluated by immunocytochemistry and confocal analysis at DIV28. First, the efficiency of transfection was tested by Kal7 immunostaining in Myc-His and Myc-His-Kal7 transfected cultures (Supplementary Material, Fig. S4A). As expected, endogenous levels of Kal7 in Myc-His-transfected R6/1 cortical neurons were significantly lower ($P < 0.05$) than those in WT neurons. In contrast, similar Kal7 immunostaining was found between WT and R6/1 cortical cultures overexpressing Kal7, demonstrating similar transfection efficiency (Supplementary Material,

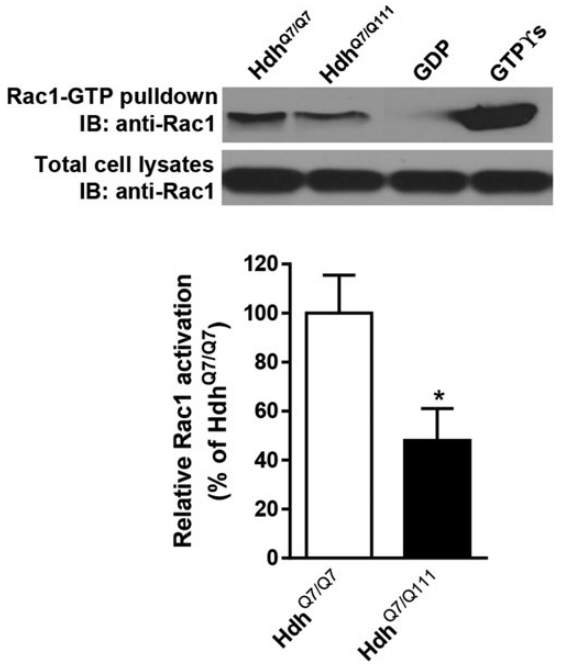

Figure 9. Rac1 activity is reduced in the cortex of $Hdh^{Q7/Q111}$ mice. Representative western blot of cortical extracts isolated from WT $Hdh^{Q7/Q7}$ and mutant $Hdh^{Q7/Q111}$ mice at 8 months of age showing Rac1-GTP and total Rac1 levels. Activated (GTP-bound) Rac1 was detected by immunoblotting of pull-down experiments from cortical extracts. Diminished Rac1 activity was found in $Hdh^{Q7/Q111}$ mutant mice compared with $Hdh^{Q7/Q7}$ WT mice ($n = 5$ animals per genotype), whereas similar total Rac1 levels were found between genotypes. Histograms represent mean ± SEM and are expressed as percentage of WT animals. Student's two-tailed t test was performed. *$P < 0.05$ compared with $Hdh^{Q7/Q7}$ mice.

Fig. S4A). Next, cell survival was determined to rule out that genotype or transfection condition could affect synapse number. No significant changes in neuronal density were found between WT and HD cortical cultures (Supplementary Material, Fig. S4B).

Then, the density of excitatory synapses, as the number of Vglut1 and PSD-95 positive coclusters, was examined (Fig. 11). A severe reduction in the density of excitatory synapses, evidenced by a significant decline ($P < 0.001$) in PSD-95, Vglut1 and PSD-95/Vglut1 positive coclusters, was found in Myc-His-transfected R6/1 cortical neurons compared with Myc-His-transfected WT neurons. Importantly, when Vglut1 and PSD-95 positive clusters were analyzed in WT and R6/1 cortical neurons transfected with exogenous Kal7 (Myc-His-Kal7), no significant differences between genotypes were observed. Moreover, we found that almost every Vglut1 cluster was apposed to a PSD-95 cluster, proving similar density of Vglut1 and PSD95 positive coclusters in both neuronal genotypes. Altogether, these findings suggest an important contribution of dysfunctional Kal7 in cortical structural plasticity alterations in HD mice.

Discussion

Cognitive dysfunction involving psychomotor, emotional, attentional and executive functions has been reported in asymptomatic HD gene carriers, years before the onset of motor symptoms (6,37–39,53–55). Although there is disparity in the nature and evolution of such cognitive decline, most evidence indicates that these early cognitive changes stem from corticostriatal circuit dysfunction rather than from striatal or cortical neuronal degeneration (56,57). However, it is not clear whether (i) striatal dysfunction develops first involving thereafter other brain regions namely the neocortex or the limbic system, (ii) whether atrophy of pyramidal cortical neurons with the consequent loss of cortical projections is the primary cause of the striatal pathology or (iii) whether both cortical and striatal changes progress in parallel inducing dysfunction of the corticostriatal pathway. In this study, we aimed to determine the sequence of brain region pathology involved in corticostriatal-dependent cognitive deficits in HD mice and the molecular mechanisms underlying such impairments.

We have demonstrated in two different HD mouse models: $Hdh^{Q7/Q111}$ knock-in mice and transgenic exon-1 R6/1 mice, motor learning deficits in the accelerated rotarod that were evident at 2 months of age worsening thereafter. Importantly, at early and middle disease stages, these mice do not display decreased motor coordination function evidenced by similar performance in the fixed rotarod or the open field compared with WT mice. Moreover, both HD mouse models also exhibited procedural learning deficits at ages in which motor coordination is not impaired. Interestingly, motor learning disturbances appear in HD mice months before hippocampal-dependent cognitive impairments (58–60), indicating that alterations in the corticostriatal pathway precede hippocampal dysfunction in these HD mice. These results are in agreement with previous data in YAC128 mice showing altered motor learning in the rotarod task before any other behavioral abnormality (61), and with data in humans in which deficits in procedural learning are among the earliest cognitive symptoms that can be detected (6,38,54,62–65). Consistent with corticostriatal-dependent cognitive deficits, we also demonstrated impaired corticostriatal LTP in 2-month-old $Hdh^{Q7/Q111}$ knock-in mice, an age in which motor and procedural learning start to decline, supporting the idea that these cognitive deficits come from functional changes in the corticostriatal circuits. In fact, abnormal corticostriatal activity has already been reported in YAC128 and R6/2 mice (12,66,67).

Morphological and/or biochemical alterations either in pyramidal neurons from the neocortex or from the striatum may be responsible for the early cognitive and synaptic deficits observed in HD mice. Dendritic spine pathology analyzed by Golgi staining in striatal spiny neurons and pyramidal cortical neurons has been previously reported at late disease stages in different HD mouse models and in brains from HD patients (3,19,20,23,68). Interestingly, in this work, we reported for the first time an early and specific decrease in dendritic spine density and a shift in spine distribution in cortical pyramidal neurons from the motor cortex of $Hdh^{Q7/Q111}$ mice without evident structural changes in the striatum that associate with the initial detection of corticostriatal-dependent learning deficits as well as with alterations in corticostriatal synaptic plasticity. Moreover, a moderate cortical-specific reduction in spinophilin-positive puncta was also demonstrated in $Hdh^{Q7/Q111}$ knock-in mice, suggesting that corticostriatal pathology could involve early structural synaptic changes in the cortex that would compromise striatal function. In agreement with our data, a recent work by Murmu *et al.* (69) has described reduced spine survival and density at presymptomatic phases in R6/2 mice when no motor coordination and balance deficits are observed, suggesting that synaptic dysfunction precedes the motor symptoms in HD. Overall, these data indicate that loss of dendritic spines at early HD disease stages is a common feature manifested in both KI and R6 lines.

Given the importance of the glutamatergic inputs to the functioning of the cortex itself and the striatum, the next question was whether changes in glutamatergic synapses could also contribute to corticostriatal pathology. PSD-95 is exclusively

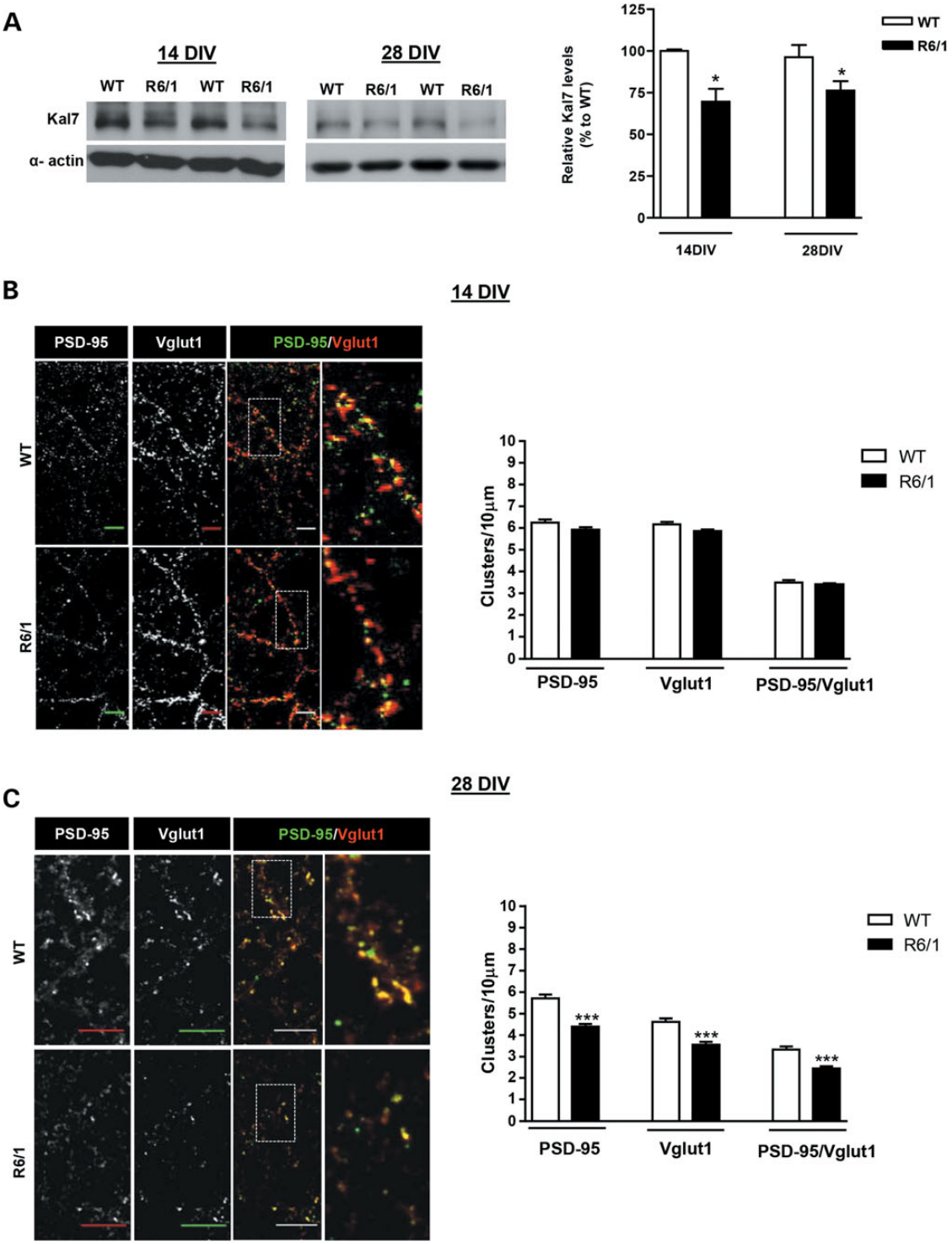

Figure 10. Reduced levels of Kal7 associates with decreased number of synapse in mature cortical neurons from R6/1 mice. (**A**) Representative western blot showing Kal7 and α-actin as loading control in cortical neurons from WT and R6/1 mice at DIV14 ($n = 3$–8 animals per genotype) and DIV28 ($n = 7$–9 animals per genotype). A significant reduction in Kal7 levels was found in mutant R6/1 cortical neurons compared with WT cortical neurons at both DIV stages. Statistical analysis was performed using Student's two-tailed *t* test. *$P < 0.05$ compared with WT cortical neurons. (**B** and **C**) Representative confocal images showing Vglut1, PSD-95 and Vglut1 (red)/PSD-95 (green) positive clusters in WT and R6/1 cortical neurons. Cortical cultures were prepared from E18.5 WT ($n = 3$) and R6/1 ($n = 5$) embryos and triplicate cultures were fixed at DIV14 (B) and DIV28 (C). Clusters of Vglut1 and PSD-95 staining were quantified along the dendrite, and the number of excitatory synapses was measured as Vglut1/PSD-95 positive clusters. Differences in the number of excitatory synapses between WT and HD neurons were only detected at DIV28 (C) but not at DIV14 (B). Quantitative analysis of Vglut1, PSD-95 and Vglut1/PSD-95 positive clusters is shown as mean ± SEM [DIV14: $n = 89$ neurons (two dendrites/each neuron) from three WT mice (three replicates/animal); $n = 149$ neurons (two dendrites/each neuron) from five R6/1 mice (three replicates/animal); DIV28: $n = 65$ neurons (two dendrites/each neuron) from three WT mice (three replicates/animal); $n = 89$ neurons (two dendrites/each neuron) from five R6/1 mice (three replicates/animal)]. Scale bar, 10 µm. ***$P < 0.01$.

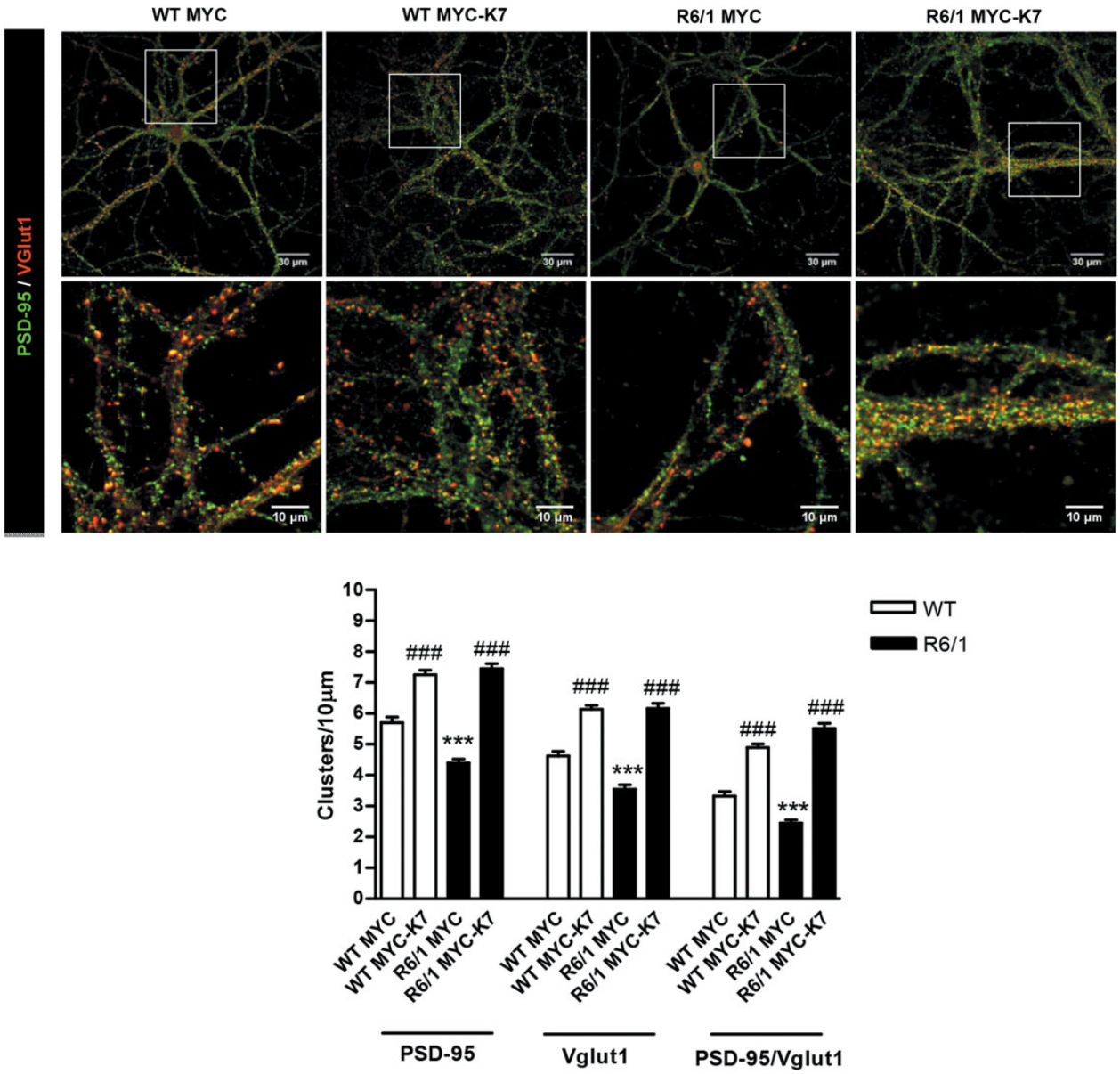

Figure 11. Exogenous expression of Kal7 restores the number of excitatory synapses in HD mature cortical neurons. Representative confocal images showing Vglut1 (red), PSD-95 (green) and Vglut1/PSD-95 positive clusters in WT and R6/1 cortical neurons transfected with Myc-His (MYC) or Myc-His-Kal7 (MYC-K7) vectors. Quantitative analysis of Vglut1, PSD-95 and Vglut1/PSD-95 positive clusters is shown as mean ± SEM [$n = 65$ neurons (two dendrites/each neuron) from three WT mice (three replicates/animal); $n = 87–89$ neurons (two dendrites/each neuron) from four R6/1 mice (three replicates/animal)]. Overexpression of Myc-K7 restores the number of PSD-95, Vglut1 and Vglut1/PSD95 positive clusters (excitatory synapses) in R6/1 cortical neurons. Statistical analysis was performed using one-way ANOVA with *post hoc* Bonferroni's multiple comparison test. $^{***}P < 0.001$ compared with WT Myc. $^{###}P < 0.001$ compared with the corresponding (WT or R6/1) Myc-control.

localized to PSD of glutamatergic excitatory synapses (70,71), where its clustering is critical for synapse function (72,73) controlling synaptic strength and activity-mediated synapse stabilization (74–76). Therefore, the number of PSD-95 clusters was analyzed in the motor cortex and dorsal striatum of $Hdh^{Q7/Q111}$ knock-in mice as a measure of postsynaptic excitatory structures. A significant reduction of PSD-95 positive clusters was found in layers I and II–III of the motor cortex of $Hdh^{Q7/Q111}$ mutant mice at 2 months of age without any major change in the striatum until 8 months of age, when the changes in cortical PSD-95 positive clusters are even more severe and also involve layer V. These findings support the hypothesis that changes in glutamatergic cortical circuits could induce altered corticocortical connectivity triggering striatal dysfunction without prominent morphological or structural changes in the striatum. Actually, cortical pyramidal neurons from layers II–III and V of sensorimotor cortex are the most prominent glutamatergic inputs to other cortical layers and dorsolateral (DL) striatum (77). Consistent with our hypothesis, a recent study has demonstrated that specific reduction of mutant huntingtin in cortical pyramidal neurons ameliorates motor and psychiatric-like behaviors as well as striatal synaptic deficits in BACHD mice (78). Moreover, it has been reported that cortical pyramidal neurons from 3-week-old R6/2 transgenic mice have decreased glutamate receptor-mediated currents (12) while deficits in learning-dependent cortical plasticity have been demonstrated

in presymptomatic R6/1 mice (2,13) and abnormal motor cortex plasticity in HD gene carriers (79).

We next addressed the potential mechanisms underlying the specific decrease of cortical PSD-95-positive excitatory synapses in HD mice at early disease stages. Kal7 is a brain-specific RhoGEF enriched in the PSD of excitatory synapses, where it plays a role in synaptic structure and function through modulation of the actin cytoskeleton dynamics (28–30,80,81). Thus, Kal7 KO mice exhibit a 30% reduction in the density of glutamatergic synapses in the CA1 hippocampal neurons while the number of Vglut1–PSD95 positive clusters in Kal7 KO cortical neurons was decreased by almost a 40% (29). Importantly, such changes were along with a decline in the magnitude of the LTP and with impaired contextual fear learning. Our results showing an early reduction of Kal7 in the cortex but not in the striatum of HD mutant mice without any change in the levels of glutamate receptors or other synaptic scaffolding proteins strongly supports a role of Kal7 in the structural synaptic changes found in the cortex of HD mice and underscores Kal7 as a candidate to mediate HD corticostriatal synaptic plasticity and behavioral deficits. In this view and given (i) the role of Kalirin as an essential factor to maintain hippocampal pyramidal neuron dendrites and dendritic spines (28) and (ii) the previously reported hippocampal deficits observed in both R6/1 and $Hdh^{Q7/Q111}$ mutant mice (58,59) would be interesting to address the role of Kal7 in HD hippocampal pathology. Indeed, mice lacking Kal7 expression show decreased hippocampal spine density and deficient hippocampal LTP while dendritic spine disturbances found in schizophrenic postmortem cortices and in the cortices and hippocampus of Alzheimer's disease patients has been associated with reduced levels of Kal7 (29,82,83–86).

Our *in vitro* findings using cortical neuronal cultures from HD mice strengthen the idea that Kal7 is involved in cortical HD synaptic pathology. Thus, decreased levels of Kal7 in HD mutant cortical neurons were associated with a significant reduction in excitatory synapses. The fact that the decrease in Kal7 can be observed in mutant cortical neurons at DIV14 and DIV28, but the reduction in excitatory contacts only at DIV28 strongly supports the idea that dendritic spines are normally developed in the absence of Kal7 but lost thereafter in accordance with a role of Kal7 in the maturation or maintenance of dendritic spines (29).

The restorative effect of Kal7 overexpression in excitatory synapses raises the question of how deficient Kal7 activity could induce synaptic alterations in HD mice. Kal7 is a well-known activator of Rac1 (26,87,88). Thus, following neuronal activity, Kal7 induces Rac1 activation that in turn causes a rapid enlargement of existing spine heads (26,87,89). Consistent with a role for deficient Kal7/Rac1 signaling in HD cortical pathology, Rac1 activity was significantly reduced in the cortex of HD mice, suggesting that decreased Rac1 function as a consequence of diminished Kal7 expression could contribute to reducing excitatory PSD-95 structures in the cortex of HD mice. These results are in agreement with previous data showing that Kalirin loss in KALRN-KO mice produces a specific reduction in cortical Rac1-GTP levels (33).

Our data cannot rule out that alterations in other GEF proteins that also regulate Rac1 activity or a contribution of Rac-1 glia dysfunction would also participate in HD synaptic pathology by reducing Rac1 activity. However, we would like to emphasize that Kal7 protein expression is absent in glia cells (88), which is the major Rac-GEF protein expressed in the cortex of adult animals (90), suggesting altogether that the reduction of Rac1 activity observed in $Hdh^{Q7/Q111}$ mice is likely related with a decrease in neuronal Kal7 levels.

Overall, in the present study, we demonstrate corticostriatal-dependent learning deficits in HD mice at early disease stages associated with deficits in corticostriatal synaptic transmission, reduction in cortical dendritic spine density and decreased cortical excitatory postsynaptic structures. These data support the concept that early morphological and biochemical changes in the cortex would be critical for triggering striatal dysfunction and the consequent HD behavioral and synaptic deficits in the absence of major structural alterations in the striatum. In the quest to elucidate the molecular pathway underlying these cortical disturbances, we have identified Kal7, a critical component of excitatory synapses that control structural and functional plasticity of dendritic spines. Altogether, our data suggest that therapeutic strategies aimed to restore cortical Kal7 activity merit particular investigation to treat synaptic dysfunction in HD.

Materials and Methods

HD mouse models

Hdh^{Q7} WT mice with 7 CAG repeats and Hdh^{Q111} knock-in mice, with targeted insertion of 109 CAG repeats that extends the glutamine segment in murine huntingtin to 111 residues, were maintained on a C57BL/6 genetic background. Male and female $Hdh^{Q7/Q111}$ heterozygous mice were intercrossed to generate age-matched $Hdh^{Q7/Q111}$ heterozygous and $Hdh^{Q7/Q7}$ WT littermates. R6/1 mice expressing exon-1 of mutant huntingtin were obtained from Jackson Laboratory (Bar Harbor, ME, USA) and maintained in a B6CBA background. Our R6/1 colony has 145 CAG repeats (91). WT littermate animals were used as the control group. All mice used in the present study were males and were housed together in numerical birth order in groups of mixed genotypes, and data were recorded for analysis by microchip mouse number. The animals were housed with access to food and water *ad libitum* in a colony room kept at 19–22°C and 40–60% humidity, under a 12:12 h light/dark cycle. All procedures were performed in compliance with the National Institutes of Health Guide for the Care and Use of Laboratory Animals, and approved by the local animal care committee of the Universitat de Barcelona (99/01) and Generalitat de Catalunya (00/1094), in accordance with the Directive 2010/63/EU of the European Commission.

Postmortem brain tissue

Samples of human cortex (four controls and six HD patients) and putamen (five controls and five HD patients) were obtained from Banc de Teixits Neurològics (Servei Científico-Tècnic, Universitat de Barcelona, Barcelona, Spain) following the guidelines of the local ethics committees [controls (mean ± SEM; age: 53.5 ± 6.8 years; postmortem intervals of 4–18 h), HD brain grades 3 and 4 (mean ± SEM; age: 54.5 ± 6.5 years; postmortem intervals of 4–17 h)]. All the ethical guidelines contained within the latest Declaration of Helsinki were taken into consideration, and informed consent was obtained from all subjects under study.

Behavioral assessment

Accelerating rotarod training procedure

Independent cohorts of 1-, 2-, 6- and 8-month-old $Hdh^{Q7/Q7}$ and $Hdh^{Q7/Q111}$ animals ($n = 9$–14 per genotype, only males) and 1-, 2- and 3-month-old WT and R6/1 animals ($n = 9$–14 per genotype, only males) were used. For the accelerating task, mice were placed on a motorized rod (30 mm diameter). The rotation speed gradually increased from 4 to 40 rpm over the course of 5 min. The time latency was recorded when the animal was

unable to keep up with the increasing speed and fell (42,95). Accelerating rotarod training procedure training/testing was performed four times per day for three consecutive days. Different trials during the same day were separately by 1 h.

Swimming T-Maze test of strategy shifting

Independent cohorts of 6-month-old $Hdh^{Q7/Q7}$ and $Hdh^{Q7/Q111}$ animals ($n = 11–19$ per genotype, only males) and 2-month-old WT and R6/1 animals ($n = 11–19$ per genotype, only males) were used. The T-maze apparatus used was a glass maze consisting of three arms, two of them situated at 180° from each other and the third, representing the stem arm of the T, situated at 90° with respect to the other two. All arms were 45 cm long, 8 cm wide and enclosed by a transparent 20 cm wall. Six-month-old male mice were trained to swim from the stem arm of the T to the other arms. In one of them, there was a transparent escape platform, covered by water. During the acquisition phase of swimming T-maze of strategy shifting (two consecutive days—first day: eight trials; second day: four trials), each mouse was placed in the water, allowed to swim until they reach the platform, and the latency and errors (1: error, 0: non-error) to reach the platform were recorded. Swimming to the platform was arbitrarily given a score of 0, whereas swimming away from the platform was given a score of 1. Based on this criterion, to successfully complete the task, mice should remember the location or the path to the escape platform, that is, to get a score of 0. The mice have to be able to find the platform and learn the strategy faster across trials. After the acquisition phase, we changed the location of the platform to the opposite arm. During the reversal phase of Swimming T-maze of strategy shifting (2 consecutive days—second day: four trials; third day: eight trials), mice were placed in the water, and the latency and errors were recorded until they reach the platform. Different trials during the same day were categorized by 1 h.

Fixed rotarod

For rotarod learning, independent cohorts of 2-, 6- and 8-month-old $Hdh^{Q7/Q7}$ and $Hdh^{Q7/Q111}$ mice ($n = 9–15$ per genotype, only males) were trained at a fixed speed of 10 rpm and subsequently tested with two trials per day spaced 1–2 h apart during three consecutive days (92). During this learning phase, mice falling from the rod were returned, and the number of falls was recorded until the addition of the latencies to fall reached a total time of 60 s per trial. The testing was performed at 5 (data not shown), 10 and 25 rpm, and the number of falls was recorded in a period of 60 s.

Open field

Independent cohorts of 2-, 6- and 8-month-old $Hdh^{Q7/Q7}$ and $Hdh^{Q7/Q111}$ animals ($n = 8–14$ per genotype, only males) were used. The device consisted of a white circular arena with 40 cm diameter and 40 cm high. The light intensity was 40 lux throughout the arena, and the room temperature was kept at 19–22°C and 40–60% humidity. Mice were placed into the arena during two consecutive days (15 min/day) and spontaneous locomotor activity was measured as total distance traveled. The arena was rigorously cleaned between animals in order to avoid odors. Animals were tracked and recorded with SMART Junior Software.

Electrophysiology

Corticostriatal synaptic transmission

Coronal brain slices (450 μm thickness) were prepared from mice ($n = 7–8$ slices per genotype, only males) as described previously (93) and incubated for 1 h at room temperature (21–24°C) in artificial cerebrospinal fluid (aCSF). The aCSF contained (in mM) NaCl 124, KCl 2.69, KH_2PO_4 1.25, $MgSO_4$ 2, $NaHCO_3$ 26, $CaCl_2$ 2 and glucose 10, and was gassed with 95% O_2 and 5% CO_2. Brain slices containing both striatum and cortex were transferred to an immersion recording chamber and superfused (2.5 ml/min) with gassed aCSF warmed to 32–34°C. After 1 h of equilibration, extracellular field potentials were recorded in the dorsomedial (DM) striatum by a glass microelectrode filled with 1 M NaCl on stimulation of the white matter between the cortex and the striatum with a bipolar tungsten electrode via a 2100 isolated pulse stimulator (A-M Systems, Inc.). LTP was induced by applying tetanic stimulation twice (four 1 s, 100 Hz trains delivered every 10 s) at an interval of 10 min, and potentiation was measured for 1 h after LTP induction at 0.1 Hz. For each experiment, PS amplitude was expressed as a percentage of average pre-tetanus baseline amplitude. Data were stored on a Pentium-based PC using a PowerLab 4/26 acquisition system (AD Instruments, Bella Vista, Australia); Scope software (AD Instruments) was used to display PS and measurements of the amplitude of PSs. Statistical differences, compared with pre-tetanus baseline amplitude values, were established using the two-tailed Student's *t*-test.

Dendritic spine assessment and confocal analysis

Cortical and striatal neurons from 2-month-old $Hdh^{Q7/Q7}$ and $Hdh^{Q7/Q111}$ mice ($n = 5$ per genotype, only males) were labeled using the Helios Gene Gun System (Bio-Rad), as previously described (58,93,94). Briefly, a suspension containing 3 mg of 1,1′-dioctadecyl-3,3,3′,3′-tetramethylindocarbocyanine perchlorate (DiI) (Molecular Probes, Invitrogen) dissolved in 100 μl of methylene chloride (Sigma-Aldrich) and mixed with 50 mg of tungsten particles (1.7 mm diameter; Bio-Rad) was spread on a glass slide and air-dried. The mixture was resuspended in 3.5 ml distilled water and sonicated. Subsequently, the mixture was drawn into Tefzel tubing (Bio-Rad) and then removed to allow tube drying for 5 min under a flow of nitrogen gas. The tube was then cut into 13 mm pieces to be used as gene gun cartridges. Dye-coated particles were delivered to 200 μm coronal sections containing both cortex and striatum at 80 psi through a membrane filter of 3 μm pore size and 8×10 pores/cm^2 (Millipore, Temecula, CA). Sections were stored at room temperature in phosphate buffered saline (PBS) for 3 h protected from light and then incubated with Hoechst 33258, and mounted in Mowiol to be analyzed. DiI-labeled pyramidal neurons from motor cortex (M1) and medium spiny neurons from dorsal striatum were imaged using a Leica Confocal SP5 with a ×63 oil-immersion objective. Conditions such as pinhole size (1 AU) and frame averaging (four frames per z-step) were held constant throughout the study. Confocal z-stacks were taken with a digital zoom of 5, a z-step of 0.2 μm and 1024×1024 pixel resolution, yielding an image with pixel dimensions of 49.25×49.25 μm. z-Stacks were deconvolved using the Acolomo plugins from ImageJ, to improve voxel resolution and reduce optical aberration along the z-axis. Segments of apical dendrites from cortical pyramidal neurons and dendrites from striatal medium spiny neurons were selected for analysis of spine density according to the following criteria: (i) segments with no overlap with other branches that would obscure visualization of spines and (ii) segments either 'parallel' to or 'at acute angles' relative to the coronal surface of the section to avoid ambiguous identification of spines. Only spines arising from the lateral surfaces of the dendrites were included in the study; spines located on the top or bottom of the dendrite surface were ignored. Spine density was measured manually in the

stacks using the ImageJ Plugin Cell Counter. Spines were marked in the appropriate focal plane preventing any double counting of spines. Spines were counted in dendritic segments range from 15 to 40 μm of length. Measurements of the head diameter were manually performed using the ImageJ software as described in Enrique-Barreto *et al.* (94). Briefly, a single image from the stack was selected for analysis and the scale was set. Each spine was selected, duplicated, rescaled (X and Y scales were set at 25) and thresholded until only the spine was selected. The 'Polygon selections' tool was used to define the perimeter of the head, splitting it from the neck or the dendritic shaft. Area measurements and diameter were obtained from this image. The spine head diameter was analyzed as a continuous distribution. To this end, we proceeded as follows: first, all the identified spines were categorized as spines without neck (stubby spines) or with a clear neck. From the latter, blind measurements of the head diameter were performed manually using ImageJ for all the spines in control mice. Then, a distribution analysis of head diameter was performed. The Gaussian adjustment resulted in a normal distribution with a mean value of 0.711 μm for cortical (Gaussian fit $P = 0.895$) and 0.605 μm for striatal neurons (Gaussian fit $P = 0.895$). From the estimated mean value, spine populations were divided into spines with diameters below the mean average (thin spines), spines with head diameters above the mean value (mushrooms) and a third category including all the non-neck spines (stubby spines).

Brain processing and immunohistochemistry

Heterozygous mutant $Hdh^{Q7/Q111}$ and WT $Hdh^{Q7/Q7}$ mice at 2 ($n = 5$–6 per genotype) and at 8 ($n = 6$ per genotype) months of age were deeply anesthetized and immediately perfused transcardially with saline followed by 4% paraformaldehyde (PFA)/phosphate buffer. Brains were removed and postfixed overnight in the same solution, cryoprotected by immersion in 30% sucrose and then frozen in dry ice-cooled methylbutane. Serial coronal cryostat sections (30 μm) through the whole brain were collected in PBS as free-floating sections. Sections were rinsed three times in PBS and permeabilized and blocked in PBS containing 0.3% Triton X-100 and 3% normal goat serum (Pierce Biotechnology, Rockford, IL) for 15 min at room temperature. The sections were then washed in PBS and incubated overnight at 4°C with Spinophilin (1:250, Millipore) and PSD-95 (1:500, Thermo Scientific, Waltham, MA) antibodies that were detected with Cy3 anti-rabbit and Cy2 anti-mouse secondary antibodies (1:200, Jackson ImmunoResearch, West Grove, PA). As negative controls, some sections were processed as described in the absence of primary antibody and no signal was detected.

Confocal microscopy analysis and immunofluorescence-positive puncta counting

PSD-95 and spinophilin-positive spine-like structures were examined as previously described (96). The analyses were performed using a Leica Microsystems Heidelberg (Mannheim, Germany) TCS SL laser scanning confocal spectral microscope with argon and helium-neon lasers attached to a Leica DMIRE2 inverted microscope. Images were taken using a ×63 numerical aperture objective with ×4 digital zoom and standard (one Airy disc) pinhole. Three coronal sections (30 μm thick) per animal spaced 0.24 mm apart containing the motor area M1 and dorsal striatum were used. For each slice, we obtained three fields/cortical layer (I, II/III and V) of the M1 area and three fields/dorsal striatum region (DL and DM). In each field, an entire z-stack was obtained, and optical sections (three per field) of 0.5 μm were collected separately (4 μm) in order to avoid biased counting. The number and area of PSD-95 and spinophilin-positive puncta were measured using NIH ImageJ version 1.33 by Wayne Rasband (National Institutes of Health, Bethesda, MD).

To analyze either spinophilin or PSD-95 immunolabeling, brightness and contrast of fluorescence images were adjusted so that only punctate fluorescence but no weak diffuse background labeling was visible. In the article, we use the term 'puncta' and 'cluster' interchangeable to refer to discrete points of protein at the fluorescence microscope. Positive puncta/cluster within a specific field was recognized by identifying the presence of overlapping 10–100 pixels.

Western blot analysis

Heterozygous mutant $Hdh^{Q7/Q111}$, WT $Hdh^{Q7/Q7}$, R6/1 and WT mice were killed by cervical dislocation at the age of 2 or 8 months for $Hdh^{Q7/Q7}$ and $Hdh^{Q7/Q111}$ mice and 2 or 3 months for WT and R6/1 mice. Brains were quickly removed, dissected, frozen in dry ice and stored at −80°C until use. Protein extraction from striatal and cortical tissue ($n = 5$–8 per genotype, only males) and western blot analysis were performed as previously described (60). The primary antibodies used were GluA1 (1:1000, Upstate, Lake Placid, NY); GluN1 (1:500, Chemicon, Temecula, CA); GluN2B (1:1000, Cell Signaling Technology, Beverly, MA); CaMKII and Shank3 (1:500, Santa Cruz Biotechnology, Santa Cruz, CA); PSD-95 (1:1000, Thermo Scientific); Spinophilin (1:1000, Millipore); Vglut1 (1:50 000, Synaptic Systems, Göttingen, Germany), Synaptophysin (1:1000, Abcam, Cambridge, UK) and Rac1 (1:2000, BD Transduction Laboratories, San Diego, CA); Kal7 (JH2958; 1:1000) and Kalirin-spectrin antiserum (JH2582; 1:1000) (87). Loading control was performed by reproving the membranes with an antibody to α-tubulin (1:50 000, Sigma-Aldrich) or α-actin (1:20 000, MP Biochemicals, Aurora, OH). ImageJ software was used to quantify the different immunoreactive bands relative to the intensity of the α-tubulin/actin band in the same membranes within a linear range of detection for the enhanced chemiluminiscent kit reagent. Data are expressed as the mean ± SEM of band density.

Rac1 activation assay

For measurement of activated Rac1, cerebral cortex from $Hdh^{Q7/Q7}$ and $Hdh^{Q7/Q111}$ mice ($n = 5$ per genotype, only males) was rapidly homogenized in ice-cold pull-down lysis buffer containing 50 mM Tris–HCl, 1 mM ethylenediaminetetraacetic acid (EDTA), 500 mM NaCl, 10 mM $MgCl_2$, 1% Triton X-100, 0.5% sodium deoxycholate, 0.1% sodium dodecyl sulphate (SDS), 10% glycerol, 0.5% β-mercaptoethanol, plus sodium orthovanadate and protease inhibitor cocktail (Sigma-Aldrich). The lysates were centrifuged at 16 000*g* for 15 min at 4°C to remove insoluble material. Cleared lysates and positive controls were mixed with 10 μg of PAK-GST Protein Beads (Cytoskeleton Inc., Denver, CO) and incubated with shaking for 1 h at 4°C. The beads were washed three times with ice-cold pull-down lysis buffer. After the last wash, the supernatant was carefully removed and the pellet was resuspended in 20 μl of 5× sodium dodecyl sulphate-polyacrylamide gel electrophoresis sample buffer and boiled for 5 min. For positive and negative controls, 10 mM EDTA, 60 mM $MgCl_2$ and 100 μM GTPγS (positive control) or 1 mM GDP (negative control) were added and incubated with lysates for 15 min at 30°C. Rac1 bound to PAK-GST was detected by western blotting using a Rac1 antibody (1:2000, BD Transduction Laboratories).

Primary cultures of mouse cortical neurons, transfection and immunocytochemistry

Dissociated cortical cultures prepared from E18.5 WT and R6/1 embryos were plated at a density of 400 000 neurons onto 60 mm culture dishes (for biochemical analysis) or at a density of 50 000 neurons onto coverslips placed in 24-well plates (for immunocytochemical analysis) precoated with 0.1 mg/ml poly-d-lysine (Sigma Chemical Co., St. Louis, MO). Neurons were cultured in Neurobasal medium (Gibco-BRL, Renfrewshire, Scotland, UK), supplemented with B27 (Gibco-BRL) and Glutamax™ (Gibco-BRL). Cultures were maintained at 37°C in a humidified atmosphere containing 5% CO_2. Thereafter, 50% of the medium was replaced once a week for up to 4 weeks. For biochemical analyses, 14 or 28 days after plating, neurons were homogenized in cold lysis buffer [50 mM Tris base (pH 7.5), 150 mM NaCl, 2 mM EDTA, 1% NP-40] supplemented with 1 mM sodium orthovanadate and protease inhibitor cocktail (Sigma-Aldrich), cleared by centrifugation at 16 000*g* for 15 min and supernatants collected. For immunocytochemical experiments, 12 days after plating, neurons were transfected with pcDNA 3.1/myc-His (+) or pEAK. Myc.His. Kal7 (87) plasmids using Fugene transfection Reagent (Promega, Madison, WI). After 14 or 28 DIV, neurons were fixed with 4% PFA/phosphate buffer for 10 min, rinsed in PBS, blocked in PBS containing 0.1 M glycine for 10 min and permeabilized in PBS containing 0.1% saponin for 10 min and blocked in PBS containing Normal Horse Serum 15% for 30 min at room temperature. Neurons were then washed in PBS and incubated overnight at 4°C with PSD-95 (1:250, Thermo Scientific) and Vglut1 (1:500, Synaptic Systems) antibodies that were detected with Cy3 anti-mouse and Alexa647 anti-rabbit secondary antibodies (1:200, Jackson ImmunoResearch). As negative controls, some cultures were processed as described in the absence of primary antibody; no signal was detected. Immunofluorescence was analyzed by confocal microscopy using a TCS SL laser scanning confocal spectral microscope (Leica Microsystems Heidelberg). Single images were taken using a ×63 oil-immersion objective with ×1 digital zoom. Conditions such as pinhole size (1 AU) and frame averaging (four frames per z-step) were held constant throughout the study. The number of positive PSD-95, Vglut1 and PSD-95/Vglut1 positive clusters was measured using NIH ImageJ version 1.33 by Wayne Rasband (National Institutes of Health) and the NeuronJ Plugin (a Java program for Neurite Tracing and Quantification). Briefly, using NeuronJ Plugin, the tracing from at least 65–145 neurites (1–2 neurites per neuron) for each condition and in triplicate was analyzed and the number of positive PSD-95, Vglut1 and PSD-95/Vglut1 positive clusters measured per 10 µm neurite length.

Neuronal survival

Cell survival of cortical neurons at DIV28 was assessed by nuclear DNA staining with Hoechst 33258. Neurons at DIV28 were fixed as mentioned before and stained with Hoechst 33258 (1 mg/ml) for 5 min. Stained cells were then washed twice in PBS and mounted under glass coverslips with Mowiol. Neuronal survival is represented as the percentage of Hoechst-stained nuclei positive cells compared with the number of WT Myc-transfected cells. Seventy-five fields per triplicate were counted per condition.

Statistical analysis

All data are expressed as mean ± SEM. Statistical analysis was performed using the unpaired Student's *t*-test, Wald's test, one-way analysis of variance (ANOVA) or two-way ANOVA with the appropriate *post hoc* test, as indicated in the figure legends. Differences with $P < 0.05$ were considered significant.

Supplementary Material

Supplementary Material is available at *HMG* online.

Acknowledgements

We are very grateful to Ana Lopez and Maria Teresa Muñoz for technical assistance, Dr Teresa Rodrigo and the staff of the animal care facility (Facultat de Psicologia, Universitat de Barcelona), Dr Garikoitz Azkona and the staff of the animal care facility (Facultat de Medicina, Universitat de Barcelona) and Dr Maria Calvo, Anna Bosch and Elisenda Coll from the Advanced Optical Microscopy Unit from Scientific and Technological Centers from University of Barcelona for their support and advice. We are grateful to the Banc de Teixits Neurològics (Biobanc-HC-IDIBAPS) for providing human brain samples from control subjects and HD patients. We thank members of our laboratory for helpful discussion.

Conflict of Interest statement. None declared.

Funding

This work was supported by grants from Ministerio de Ciencia e Innovación (SAF2012-39142 to S.G. and SAF 2014-57160-R to J.A.) projects integrated in the Plan Nacional de I + D + I y cofinanciado el Fondo Europeo de Desarrollo Regional (FEDER); Cure Huntington's Disease Initiative (CHDI), Centro de Investigaciones Biomédicas en Red sobre Enfermedades Neurodegenerativas (CIBERNED CB06/05/0054 and CB06/05/0042); Generalitat de Catalunya, Spain (2014SGR-00968 to J.A.); National Institutes of Health (DA-23082 and DK-32948 to B.A.E.); Ministerio de Economía y Competitividad (BFU2011-26339), INCRECyT project from European Social Fund, PCyTA and JCCM to E.D.M.

References

1. Cepeda, C., Wu, N., Andre, V.M., Cummings, D.M. and Levine, M.S. (2007) The corticostriatal pathway in Huntington's disease. *Prog. Neurobiol.*, **81**, 253–271.
2. Cybulska-Klosowicz, A., Mazarakis, N.K., van Dellen, A., Blakemore, C., Hannan, A.J. and Kossut, M. (2004) Impaired learning-dependent cortical plasticity in Huntington's disease transgenic mice. *Neurobiol. Dis.*, **17**, 427–434.
3. Laforet, G.A., Sapp, E., Chase, K., McIntyre, C., Boyce, F.M., Campbell, M., Cadigan, B.A., Warzecki, L., Tagle, D.A. and Reddy, P.H. *et al.* (2001) Changes in cortical and striatal neurons predict behavioral and electrophysiological abnormalities in a transgenic murine model of Huntington's disease. *J. Neurosci.*, **21**, 9112–9123.
4. Hahn-Barma, V., Deweer, B., Durr, A., Dode, C., Feingold, J., Pillon, B., Agid, Y., Brice, A. and Dubois, B. (1998) Are cognitive changes the first symptoms of Huntington's disease? A study of gene carriers. *J. Neurol. Neurosurg. Psychiatry*, **64**, 172–177.
5. Ho, A.K., Sahakian, B.J., Brown, R.G., Barker, R.A., Hodges, J.R., Ane, M.N., Snowden, J., Thompson, J., Esmonde, T. and Gentry, R. *et al.* (2003) Profile of cognitive progression in early Huntington's disease. *Neurology*, **61**, 1702–1706.
6. Lawrence, A.D., Hodges, J.R., Rosser, A.E., Kershaw, A., ffrench-Constant, C., Rubinsztein, D.C., Robbins, T.W. and

Sahakian, B.J. (1998) Evidence for specific cognitive deficits in preclinical Huntington's disease. *Brain*, **121**, 1329–1341.
7. Paulsen, J.S., Zhao, H., Stout, J.C., Brinkman, R.R., Guttman, M., Ross, C.A., Como, P., Manning, C., Hayden, M.R. and Shoulson, I. (2001) Clinical markers of early disease in persons near onset of Huntington's disease. *Neurology*, **57**, 658–662.
8. Rosenberg, N.K., Sorensen, S.A. and Christensen, A.L. (1995) Neuropsychological characteristics of Huntington's disease carriers: a double blind study. *J. Med. Genet.*, **32**, 600–604.
9. Schneider, S.A., Wilkinson, L., Bhatia, K.P., Henley, S.M., Rothwell, J.C., Tabrizi, S.J. and Jahanshahi, M. (2010) Abnormal explicit but normal implicit sequence learning in premanifest and early Huntington's disease. *Mov. Disord.*, **25**, 1343–1349.
10. Kassubek, J., Juengling, F.D., Kioschies, T., Henkel, K., Karitzky, J., Kramer, B., Ecker, D., Andrich, J., Saft, C. and Kraus, P. *et al.* (2004) Topography of cerebral atrophy in early Huntington's disease: a voxel based morphometric MRI study. *J. Neurol. Neurosurg. Psychiatry*, **75**, 213–220.
11. Rosas, H.D., Lee, S.Y., Bender, A.C., Zaleta, A.K., Vangel, M., Yu, P., Fischl, B., Pappu, V., Onorato, C. and Cha, J.H. *et al.* (2010) Altered white matter microstructure in the corpus callosum in Huntington's disease: implications for cortical "disconnection". *Neuroimage*, **49**, 2995–3004.
12. Andre, V.M., Cepeda, C., Venegas, A., Gomez, Y. and Levine, M.S. (2006) Altered cortical glutamate receptor function in the R6/2 model of Huntington's disease. *J. Neurophysiol.*, **95**, 2108–2119.
13. Mazarakis, N.K., Cybulska-Klosowicz, A., Grote, H., Pang, T., van Dellen, A., Kossut, M., Blakemore, C. and Hannan, A.J. (2005) Deficits in experience-dependent cortical plasticity and sensory-discrimination learning in presymptomatic Huntington's disease mice. *J. Neurosci.*, **25**, 3059–3066.
14. Cummings, D.M., Andre, V.M., Uzgil, B.O., Gee, S.M., Fisher, Y. E., Cepeda, C. and Levine, M.S. (2009) Alterations in cortical excitation and inhibition in genetic mouse models of Huntington's disease. *J. Neurosci.*, **29**, 10371–10386.
15. Lai, K.O. and Ip, N.Y. (2013) Structural plasticity of dendritic spines: the underlying mechanisms and its dysregulation in brain disorders. *Biochim. Biophys. Acta*, **1832**, 2257–2263.
16. Shepherd, G.M. and Erulkar, S.D. (1997) Centenary of the synapse: from Sherrington to the molecular biology of the synapse and beyond. *Trends Neurosci.*, **20**, 385–392.
17. Van Der Zee, E.A. (2014) Synapses, spines and kinases in mammalian learning and memory, and the impact of aging. *Neurosci. Biobehav. Rev.*, **50**, 77–85.
18. von Bohlen Und, H.O. (2009) Structure and function of dendritic spines within the hippocampus. *Ann. Anat.*, **191**, 518–531.
19. Guidetti, P., Charles, V., Chen, E.Y., Reddy, P.H., Kordower, J.H., Whetsell, W.O. Jr, Schwarcz, R. and Tagle, D.A. (2001) Early degenerative changes in transgenic mice expressing mutant Huntingtin involve dendritic abnormalities but no impairment of mitochondrial energy production. *Exp. Neurol.*, **169**, 340–350.
20. Spires, T.L., Grote, H.E., Garry, S., Cordery, P.M., van Dellen, A., Blakemore, C. and Hannan, A.J. (2004) Dendritic spine pathology and deficits in experience-dependent dendritic plasticity in R6/1 Huntington's disease transgenic mice. *Eur. J. Neurosci.*, **19**, 2799–2807.
21. Ferrante, R.J., Kowall, N.W. and Richardson, E.P. Jr (1991) Proliferative and degenerative changes in striatal spiny neurons in Huntington's disease: a combined study using the section-Golgi method and calbindin D28k immunocytochemistry. *J. Neurosci.*, **11**, 3877–3887.
22. Graveland, G.A., Williams, R.S. and DiFiglia, M. (1985) Evidence for degenerative and regenerative changes in neostriatal spiny neurons in Huntington's disease. *Science*, **227**, 770–773.
23. Sotrel, A., Williams, R.S., Kaufmann, W.E. and Myers, R.H. (1993) Evidence for neuronal degeneration and dendritic plasticity in cortical pyramidal neurons of Huntington's disease: a quantitative Golgi study. *Neurology*, **43**, 2088–2096.
24. Govek, E.E., Newey, S.E., Akerman, C.J., Cross, J.R., Van der Veken, L. and Van Aelst, L. (2004) The X-linked mental retardation protein oligophrenin-1 is required for dendritic spine morphogenesis. *Nat. Neurosci.*, **7**, 364–372.
25. Tolias, K.F., Bikoff, J.B., Kane, C.G., Tolias, C.S., Hu, L. and Greenberg, M.E. (2007) The Rac1 guanine nucleotide exchange factor Tiam1 mediates EphB receptor-dependent dendritic spine development. *Proc. Natl Acad. Sci. USA*, **104**, 7265–7270.
26. Xie, Z., Srivastava, D.P., Photowala, H., Kai, L., Cahill, M.E., Woolfrey, K.M., Shum, C.Y., Surmeier, D.J. and Penzes, P. (2007) Kalirin-7 controls activity-dependent structural and functional plasticity of dendritic spines. *Neuron*, **56**, 640–656.
27. Zhang, H., Webb, D.J., Asmussen, H., Niu, S. and Horwitz, A.F. (2005) A GIT1/PIX/Rac/PAK signaling module regulates spine morphogenesis and synapse formation through MLC. *J. Neurosci.*, **25**, 3379–3388.
28. Ma, X.M., Huang, J., Wang, Y., Eipper, B.A. and Mains, R.E. (2003) Kalirin, a multifunctional Rho guanine nucleotide exchange factor, is necessary for maintenance of hippocampal pyramidal neuron dendrites and dendritic spines. *J. Neurosci.*, **23**, 10593–10603.
29. Ma, X.M., Kiraly, D.D., Gaier, E.D., Wang, Y., Kim, E.J., Levine, E. S., Eipper, B.A. and Mains, R.E. (2008) Kalirin-7 is required for synaptic structure and function. *J. Neurosci.*, **28**, 12368–12382.
30. Ma, X.M., Wang, Y., Ferraro, F., Mains, R.E. and Eipper, B.A. (2008) Kalirin-7 is an essential component of both shaft and spine excitatory synapses in hippocampal interneurons. *J. Neurosci.*, **28**, 711–724.
31. Penzes, P., Johnson, R.C., Sattler, R., Zhang, X., Huganir, R.L., Kambampati, V., Mains, R.E. and Eipper, B.A. (2001) The neuronal Rho-GEF Kalirin-7 interacts with PDZ domain-containing proteins and regulates dendritic morphogenesis. *Neuron*, **29**, 229–242.
32. Ma, X.M., Huang, J.P., Kim, E.J., Zhu, Q., Kuchel, G.A., Mains, R. E. and Eipper, B.A. (2011) Kalirin-7, an important component of excitatory synapses, is regulated by estradiol in hippocampal neurons. *Hippocampus*, **21**, 661–677.
33. Cahill, M.E., Xie, Z., Day, M., Photowala, H., Barbolina, M.V., Miller, C.A., Weiss, C., Radulovic, J., Sweatt, J.D. and Disterhoft, J.F. *et al.* (2009) Kalirin regulates cortical spine morphogenesis and disease-related behavioral phenotypes. *Proc. Natl Acad. Sci. USA*, **106**, 13058–13063.
34. Cahill, M.E., Jones, K.A., Rafalovich, I., Xie, Z., Barros, C.S., Muller, U. and Penzes, P. (2012) Control of interneuron dendritic growth through NRG1/erbB4-mediated kalirin-7 disinhibition. *Mol. Psychiatry*, **17**, 99–107.
35. Colomer, V., Engelender, S., Sharp, A.H., Duan, K., Cooper, J.K., Lanahan, A., Lyford, G., Worley, P. and Ross, C.A. (1997) Huntingtin-associated protein 1 (HAP1) binds to a Trio-like polypeptide, with a rac1 guanine nucleotide exchange factor domain. *Hum. Mol. Genet.*, **6**, 1519–1525.
36. Backman, L., Robins-Wahlin, T.B., Lundin, A., Ginovart, N. and Farde, L. (1997) Cognitive deficits in Huntington's disease are predicted by dopaminergic PET markers and brain volumes. *Brain*, **120**, 2207–2217.

37. Foroud, T., Siemers, E., Kleindorfer, D., Bill, D.J., Hodes, M.E., Norton, J.A., Conneally, P.M. and Christian, J.C. (1995) Cognitive scores in carriers of Huntington's disease gene compared to noncarriers. *Ann. Neurol.*, **37**, 657–664.
38. Lawrence, A.D., Watkins, L.H., Sahakian, B.J., Hodges, J.R. and Robbins, T.W. (2000) Visual object and visuospatial cognition in Huntington's disease: implications for information processing in corticostriatal circuits. *Brain*, **123**, 1349–1364.
39. Lemiere, J., Decruyenaere, M., Evers-Kiebooms, G., Vandenbussche, E. and Dom, R. (2004) Cognitive changes in patients with Huntington's disease (HD) and asymptomatic carriers of the HD mutation—a longitudinal follow-up study. *J. Neurol.*, **251**, 935–942.
40. Watkins, L.H., Rogers, R.D., Lawrence, A.D., Sahakian, B.J., Rosser, A.E. and Robbins, T.W. (2000) Impaired planning but intact decision making in early Huntington's disease: implications for specific fronto-striatal pathology. *Neuropsychologia*, **38**, 1112–1125.
41. Xu, T., Yu, X., Perlik, A.J., Tobin, W.F., Zweig, J.A., Tennant, K., Jones, T. and Zuo, Y. (2009) Rapid formation and selective stabilization of synapses for enduring motor memories. *Nature*, **462**, 915–919.
42. Yang, G., Pan, F. and Gan, W.B. (2009) Stably maintained dendritic spines are associated with lifelong memories. *Nature*, **462**, 920–924.
43. Kim, J., Bordiuk, O.L. and Ferrante, R.J. (2011) Experimental models of HD and reflection on therapeutic strategies. *Int. Rev. Neurobiol.*, **98**, 419–481.
44. Anglada-Huguet, M., Xifro, X., Giralt, A., Zamora-Moratalla, A., Martin, E.D. and Alberch, J. (2014) Prostaglandin E2 EP1 receptor antagonist improves motor deficits and rescues memory decline in R6/1 mouse model of Huntington's disease. *Mol. Neurobiol.*, **49**, 784–795.
45. Allen, P.B., Ouimet, C.C. and Greengard, P. (1997) Spinophilin, a novel protein phosphatase 1 binding protein localized to dendritic spines. *Proc. Natl Acad. Sci. USA*, **94**, 9956–9961.
46. Muly, E.C., Smith, Y., Allen, P. and Greengard, P. (2004) Subcellular distribution of spinophilin immunolabeling in primate prefrontal cortex: localization to and within dendritic spines. *J. Comp. Neurol.*, **469**, 185–197.
47. Hao, J., Janssen, W.G., Tang, Y., Roberts, J.A., McKay, H., Lasley, B., Allen, P.B., Greengard, P., Rapp, P.R. and Kordower, J.H. *et al.* (2003) Estrogen increases the number of spinophilin-immunoreactive spines in the hippocampus of young and aged female rhesus monkeys. *J. Comp. Neurol.*, **465**, 540–550.
48. Tang, Y., Janssen, W.G., Hao, J., Roberts, J.A., McKay, H., Lasley, B., Allen, P.B., Greengard, P., Rapp, P.R. and Kordower, J.H. *et al.* (2004) Estrogen replacement increases spinophilin-immunoreactive spine number in the prefrontal cortex of female rhesus monkeys. *Cereb. Cortex*, **14**, 215–223.
49. Bourne, J.N. and Harris, K.M. (2008) Balancing structure and function at hippocampal dendritic spines. *Annu. Rev. Neurosci.*, **31**, 47–67.
50. Reiner, A., Albin, R.L., Anderson, K.D., D'Amato, C.J., Penney, J. B. and Young, A.B. (1988) Differential loss of striatal projection neurons in Huntington disease. *Proc. Natl Acad. Sci. USA*, **85**, 5733–5737.
51. Vonsattel, J.P. and DiFiglia, M. (1998) Huntington disease. *J. Neuropathol. Exp. Neurol.*, **57**, 369–384.
52. Lemtiri-Chlieh, F., Zhao, L., Kiraly, D.D., Eipper, B.A., Mains, R. E. and Levine, E.S. (2011) Kalirin-7 is necessary for normal NMDA receptor-dependent synaptic plasticity. *BMC Neurosci.*, **12**, 126.
53. Josiassen, R.C., Curry, L.M. and Mancall, E.L. (1983) Development of neuropsychological deficits in Huntington's disease. *Arch. Neurol.*, **40**, 791–796.
54. Lawrence, A.D., Sahakian, B.J., Hodges, J.R., Rosser, A.E., Lange, K.W. and Robbins, T.W. (1996) Executive and mnemonic functions in early Huntington's disease. *Brain*, **119**, 1633–1645.
55. Lemiere, J., Decruyenaere, M., Evers-Kiebooms, G., Vandenbussche, E. and Dom, R. (2002) Longitudinal study evaluating neuropsychological changes in so-called asymptomatic carriers of the Huntington's disease mutation after 1 year. *Acta Neurol. Scand.*, **106**, 131–141.
56. Cepeda, C., Starling, A.J., Wu, N., Nguyen, O.K., Uzgil, B., Soda, T., Andre, V.M., Ariano, M.A. and Levine, M.S. (2004) Increased GABAergic function in mouse models of Huntington's disease: reversal by BDNF. *J. Neurosci. Res.*, **78**, 855–867.
57. Levine, M.S., Cepeda, C., Hickey, M.A., Fleming, S.M. and Chesselet, M.F. (2004) Genetic mouse models of Huntington's and Parkinson's diseases: illuminating but imperfect. *Trends Neurosci.*, **27**, 691–697.
58. Brito, V., Giralt, A., Enriquez-Barreto, L., Puigdellivol, M., Suelves, N., Zamora-Moratalla, A., Ballesteros, J.J., Martin, E. D., Dominguez-Iturza, N. and Morales, M. *et al.* (2014) Neurotrophin receptor p75NTR mediates Huntington's disease-associated synaptic and memory dysfunction. *J. Clin. Invest.*, **124**, 4411–4428.
59. Giralt, A., Saavedra, A., Carreton, O., Xifro, X., Alberch, J. and Perez-Navarro, E. (2011) Increased PKA signaling disrupts recognition memory and spatial memory: role in Huntington's disease. *Hum. Mol. Genet.*, **20**, 4232–4247.
60. Giralt, A., Puigdellivol, M., Carreton, O., Paoletti, P., Valero, J., Parra-Damas, A., Saura, C.A., Alberch, J. and Gines, S. (2012) Long-term memory deficits in Huntington's disease are associated with reduced CBP histone acetylase activity. *Hum. Mol. Genet.*, **21**, 1203–1216.
61. Van Raamsdonk, J.M., Pearson, J., Slow, E.J., Hossain, S.M., Leavitt, B.R. and Hayden, M.R. (2005) Cognitive dysfunction precedes neuropathology and motor abnormalities in the YAC128 mouse model of Huntington's disease. *J. Neurosci.*, **25**, 4169–4180.
62. Gabrieli, J.D., Stebbins, G.T., Singh, J., Willingham, D.B. and Goetz, C.G. (1997) Intact mirror-tracing and impaired rotary-pursuit skill learning in patients with Huntington's disease: evidence for dissociable memory systems in skill learning. *Neuropsychology*, **11**, 272–281.
63. Heindel, W.C., Butters, N. and Salmon, D.P. (1988) Impaired learning of a motor skill in patients with Huntington's disease. *Behav. Neurosci.*, **102**, 141–147.
64. Heindel, W.C., Salmon, D.P., Shults, C.W., Walicke, P.A. and Butters, N. (1989) Neuropsychological evidence for multiple implicit memory systems: a comparison of Alzheimer's, Huntington's, and Parkinson's disease patients. *J. Neurosci.*, **9**, 582–587.
65. Schmidtke, K., Manner, H., Kaufmann, R. and Schmolck, H. (2002) Cognitive procedural learning in patients with fronto-striatal lesions. *Learn. Mem.*, **9**, 419–429.
66. Cepeda, C., Hurst, R.S., Calvert, C.R., Hernandez-Echeagaray, E., Nguyen, O.K., Jocoy, E., Christian, L.J., Ariano, M.A. and Levine, M.S. (2003) Transient and progressive electrophysiological alterations in the corticostriatal pathway in a mouse model of Huntington's disease. *J. Neurosci.*, **23**, 961–969.
67. Joshi, P.R., Wu, N.P., Andre, V.M., Cummings, D.M., Cepeda, C., Joyce, J.A., Carroll, J.B., Leavitt, B.R., Hayden, M.R., Levine, M.S. and Bamford, N.S. (2009) Age-dependent alterations of

corticostriatal activity in the YAC128 mouse model of Huntington disease. *J. Neurosci.*, **29**, 2414–2427.
68. DiFiglia, M. (1997) Clinical genetics, II. Huntington's disease: from the gene to pathophysiology. *Am. J. Psychiatry*, **154**, 1046.
69. Murmu, R.P., Li, W., Holtmaat, A. and Li, J.Y. (2013) Dendritic spine instability leads to progressive neocortical spine loss in a mouse model of Huntington's disease. *J. Neurosci.*, **33**, 12997–13009.
70. Cho, K.O., Hunt, C.A. and Kennedy, M.B. (1992) The rat brain postsynaptic density fraction contains a homolog of the Drosophila discs-large tumor suppressor protein. *Neuron*, **9**, 929–942.
71. Kistner, U., Wenzel, B.M., Veh, R.W., Cases-Langhoff, C., Garner, A.M., Appeltauer, U., Voss, B., Gundelfinger, E.D. and Garner, C.C. (1993) SAP90, a rat presynaptic protein related to the product of the Drosophila tumor suppressor gene dlg-A. *J. Biol. Chem.*, **268**, 4580–4583.
72. Goda, Y. and Davis, G.W. (2003) Mechanisms of synapse assembly and disassembly. *Neuron*, **40**, 243–264.
73. McAllister, A.K. (2007) Dynamic aspects of CNS synapse formation. *Annu. Rev. Neurosci.*, **30**, 425–450.
74. Ehrlich, I., Klein, M., Rumpel, S. and Malinow, R. (2007) PSD-95 is required for activity-driven synapse stabilization. *Proc. Natl Acad. Sci. USA*, **104**, 4176–4181.
75. El-Husseini, A.E., Schnell, E., Chetkovich, D.M., Nicoll, R.A. and Bredt, D.S. (2000) PSD-95 involvement in maturation of excitatory synapses. *Science*, **290**, 1364–1368.
76. Prange, O. and Murphy, T.H. (2001) Modular transport of postsynaptic density-95 clusters and association with stable spine precursors during early development of cortical neurons. *J. Neurosci.*, **21**, 9325–9333.
77. Charara, A., Sidibé, M. and Smith, Y. (2003) Basal ganglia circuitry and synaptic connectivity. In Tarsy, D., Vitek, J.L. and Lozano, A.M. (eds), *Contemporary Clinical Neurology: Surgical Treatment of Parkinson's Disease and Other Movement Disorders*. Humana Press Inc., Totowa, NJ. ISBN:978-0-89603-921-6.
78. Wang, N., Gray, M., Lu, X.H., Cantle, J.P., Holley, S.M., Greiner, E., Gu, X., Shirasaki, D., Cepeda, C. and Li, Y. *et al.* (2014) Neuronal targets for reducing mutant huntingtin expression to ameliorate disease in a mouse model of Huntington's disease. *Nat. Med.*, **20**, 536–541.
79. Orth, M., Schippling, S., Schneider, S.A., Bhatia, K.P., Talelli, P., Tabrizi, S.J. and Rothwell, J.C. (2010) Abnormal motor cortex plasticity in premanifest and very early manifest Huntington disease. *J. Neurol. Neurosurg. Psychiatry*, **81**, 267–270.
80. Penzes, P. and Remmers, C. (2012) Kalirin signaling: implications for synaptic pathology. *Mol. Neurobiol.*, **45**, 109–118.
81. Xie, Z., Cahill, M.E. and Penzes, P. (2010) Kalirin loss results in cortical morphological alterations. *Mol. Cell. Neurosci.*, **43**, 81–89.
82. Kiraly, D.D., Ma, X.M., Mazzone, C.M., Xin, X., Mains, R.E. and Eipper, B.A. (2010) Behavioral and morphological responses to cocaine require kalirin7. *Biol. Psychiatry*, **68**, 249–255.
83. Wang, X., Cahill, M.E., Werner, C.T., Christoffel, D.J., Golden, S. A., Xie, Z., Loweth, J.A., Marinelli, M., Russo, S.J., Penzes, P. and Wolf, M.E. (2013) Kalirin-7 mediates cocaine-induced AMPA receptor and spine plasticity, enabling incentive sensitization. *J. Neurosci.*, **33**, 11012–11022.
84. Hill, J.J., Hashimoto, T. and Lewis, D.A. (2006) Molecular mechanisms contributing to dendritic spine alterations in the prefrontal cortex of subjects with schizophrenia. *Mol. Psychiatry*, **11**, 557–566.
85. Murray, P.S., Kirkwood, C.M., Gray, M.C., Ikonomovic, M.D., Paljug, W.R., Abrahamson, E.E., Henteleff, R.A., Hamilton, R. L., Kofler, J.K. and Klunk, W.E. *et al.* (2012) β-Amyloid 42/40 ratio and kalirin expression in Alzheimer disease with psychosis. *Neurobiol. Aging*, **33**, 2807–2816.
86. Youn, H., Jeoung, M., Koo, Y., Ji, H., Markesbery, W.R., Ji, I. and Ji, T.H. (2007) Kalirin is under-expressed in Alzheimer's disease hippocampus. *J. Alzheimers Dis.*, **11**, 385–397.
87. Impey, S., Davare, M., Lesiak, A., Fortin, D., Ando, H., Varlamova, O., Obrietan, K., Soderling, T.R., Goodman, R.H. and Wayman, G.A. (2010) An activity-induced microRNA controls dendritic spine formation by regulating Rac1-PAK signaling. *Mol. Cell. Neurosci.*, **43**, 146–156.
88. Penzes, P., Johnson, R.C., Alam, M.R., Kambampati, V., Mains, R.E. and Eipper, B.A. (2000) An isoform of kalirin, a brain-specific GDP/GTP exchange factor, is enriched in the postsynaptic density fraction. *J. Biol. Chem.*, **275**, 6395–6403.
89. Tashiro, A., Minden, A. and Yuste, R. (2000) Regulation of dendritic spine morphology by the rho family of small GTPases: antagonistic roles of Rac and Rho. *Cereb. Cortex*, **10**, 927–938.
90. Penzes, P., Cahill, M.E., Jones, K.A. and Srivastava, D.P. (2008) Convergent CaMK and RacGEF signals control dendritic structure and function. *Trends Cell Biol.*, **18**, 405–413.
91. Giralt, A., Rodrigo, T., Martin, E.D., Gonzalez, J.R., Mila, M., Cena, V., Dierssen, M., Canals, J.M. and Alberch, J. (2009) Brain-derived neurotrophic factor modulates the severity of cognitive alterations induced by mutant huntingtin: involvement of phospholipaseCgamma activity and glutamate receptor expression. *Neuroscience*, **158**, 1234–1250.
92. Marco, S., Giralt, A., Petrovic, M.M., Pouladi, M.A., Martínez-Turrillas, R., Martínez-Hernández, J., Kaltenbach, L.S., Torres-Peraza, J., Graham, R.K. and Watanabe, M. *et al.* (2013) Suppressing aberrant GluN3A expression rescues synaptic and behavioral impairments in Huntington's disease models. *Nat. Med.*, **19**, 1030–1038.
93. Martin, E.D. and Buno, W. (2005) Stabilizing effects of extracellular ATP on synaptic efficacy and plasticity in hippocampal pyramidal neurons. *Eur. J. Neurosci.*, **21**, 936–944.
94. Enriquez-Barreto, L., Cuesto, G., Dominguez-Iturza, N., Gavilan, E., Ruano, D., Sandi, C., Fernandez-Ruiz, A., Martin-Vazquez, G., Herreras, O. and Morales, M. (2014) Learning improvement after PI3K activation correlates with de novo formation of functional small spines. *Front. Mol. Neurosci.*, **6**, 54.
95. Grutzendler, J., Tsai, J. and Gan, W.B. (2003) Rapid labeling of neuronal populations by ballistic delivery of fluorescent dyes. *Methods*, **30**, 79–85.
96. Rex, C.S., Lin, C.Y., Kramar, E.A., Chen, L.Y., Gall, C.M. and Lynch, G. (2007) Brain-derived neurotrophic factor promotes long-term potentiation-related cytoskeletal changes in adult hippocampus. *J. Neurosci.*, **27**, 3017–3029.